AMEGO

All-sky Medium Energy Gamma-ray Observatory

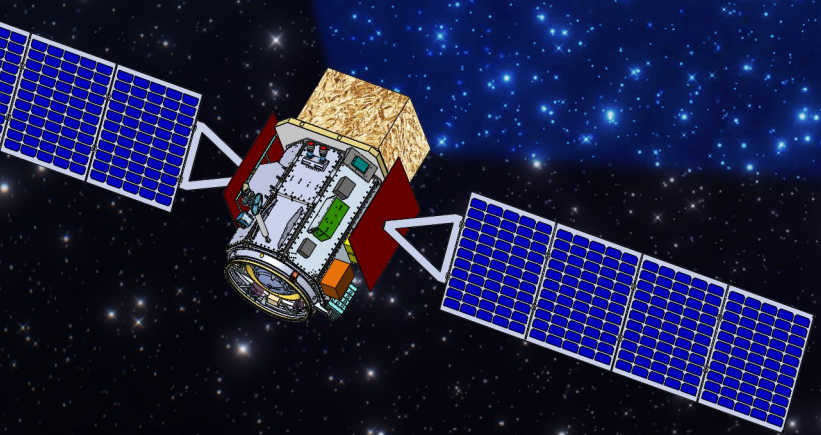

A Multimessenger Mission for the Extreme Universe

In Response to a request from the
Astro2020 Decadal Survey

Principal Investigator:
Julie McEnery
(NASA Goddard Space Flight Center)

The AMEGO Science Team:

Regina Caputo, S. Brad Cenko, Georgia De Nolfo, Alice Harding, Elizabeth Hays,
Julie McEnery (PI), John Mitchell, Jeremy Perkins, Judith Racusin, David Thompson, Tonia Venters, **(NASA/GSFC)**;
Eric Burns, Carolyn Kierans, Zorawar Wadiasingh, **(USRA/NASA/GSFC)**;
Mattia Di Mauro, Alexander Moiseev, Elizabeth Ferrara, Sean Griffin, John Krizmanic, Amy Lien, Michela Negro, Roopesh Ojha, Bindu Rani, Chris Shrader, Jacob Smith, **(CRESST/NASA/GSFC)**;
Andrew Inglis, **(CUA/NASA/GSFC)**;
Jessica Metcalfe, **(Argonne National Lab)**;
Stefano Ciprini, Dario Gasparrini, Carlotta Pittori, **(ASI Space Science Data Center)**;
Luca Zampieri, **(Astronomical Observatory of Padova)**;
Aleksey Bolotnikov, **(Brookhaven National Lab)**;
Brian Grefenstette, **(California Institute of Technology)**;
Ulisses Barres, **(Centro Brasileiro de Pesquisas Fisicas)**;
Jose-Manuel Alvarez, **(Centro De Laseres Pulsados)**;
Marco Ajello, Dieter Hartmann, Lea Marcotulli, Lih-Sin The, **(Clemson University)**;
Volker Beckmann, Denis Bernard, Jean-Philippe Lenain, **(CNRS/IN2P3)**;
Christian Gouiffes, Isabelle Grenier, Philippe Laurent, **(Commissariat a l'Energie Atomique)**;
Antonios Manousakis, **(Copernicus Astronomical Center)**;
Vincent Tatischeff, **(CSNSM/IN2P3)**;
Vaidehi S. Paliya, **(Deutsches Elektronen-Synchrotron (DESY))**;
Joachim Kopp, Jan Lommler, Uwe Oberlack, **(Die Johannes Gutenberg-Universitaet Mainz)**;
Naoko Kurahashi Neilson, **(Drexel University)**;
Foteini Oikonomou, **(European Southern Observatory)**;
Stefan Funk, **(Friedrich-Alexander-Universitaet Erlangen-Nuernberg)**;
Cosimo Bambi, **(Fudan University)**;
Sylvain Guiriec, Oleg Kargaltsev, Michael Moss, Alexander van Der Horst, George Younes, **(George Washington University)**;
Nepomuk Otte, **(Georgia Tech)**;
Daniel Castro, **(Harvard-Smithsonian CfA)**;
Yasushi Fukazawa, Tsunefumi Mizuno, Masanori Ohno, Hiromitsu Takahashi, **(Hiroshima University)**;
James Rodi, **(IAPS-INAF)**;
Natalia Auricchio, **(INAF OAS Bologna)**;
John B. Stephen, **(INAF/IASF Bologna)**;
Elisabetta Bissaldi, Leonardo Di Venere, Francesco Giordano, M. Nicola Mazziotta, **(INFN Sezione di Bari)**;
Sara Cutini, **(INFN Sezione di Perugia)**;
Stefano Dietrich, **(Institute of Atmospheric Sciences and Climate)**;
Manel Martinez , Javier Rico , **(Institut de Fisica d'Altes Energies (IFAE), The Barcelona Institute of Science and Technology (BIST))**;
Ivan Agudo, Riccardo Campana, Martina Cardillo, Ezio Caroli, Stefano Del Sordo, Andrea Giuliani, Roberto Mignani, Antonio Stamerra, **(Instituto Nazionale di Astrofisica)**;
Filippo D'Ammando, **(Istituto di Radioastronomia** & **INAF)**;
Lukasz Stawarz, **(Jagiellonian University)**;
Z. Lucas Uhm, **(Korea Astronomy and Space Science Institute)**;
Hidetoshi Kubo, **(Kyoto University)**;
Jurgen Knodlseder, Luigi Tibaldo, **(L'Observatoire Midi-Pyrenees)**;
Alexandre Marcowith, **(Laboratoire Univers et Particules de Montpellier)**;

Peter Bloser, Chris Fryer, Pat Harding, Sam Jones, Alexei V. Klimenko, Hui Li, Lucas Parker, Richard Schirato, Karl Smith, Tom Vestrand, **(Los Alamos National Lab)**;
Gottfried Kanbach, Andy Strong, **(Max Planck Institute for Extraterrestrial Physics)**;
Kazuhiro Nakazawa, Hiro Tajima, **(Nagoya University)**;
Michelle Hui, Daniel Kocveski, Colleen Wilson-Hodge, **(NASA/MSFC)**;
Teddy Cheung, Justin Finke, J. Eric Grove, Matthew Kerr, Michael Lovellette, Richard Woolf, Eric Wulf, **(Naval Research Lab)**;
Joseph Gelfand, **(New York University)**;
Markus Boettcher, **(North West University South Africa)**;
Maria Petropoulou, **(Princeton)**;
Haocheng Zhang, **(Purdue University)**;
Matthew Baring, **(Rice University)**;
Matthew Wood, Eric Charles, Seth Digel, **(SLAC National Accelerator Laboratory)**;
Vladimir Bozhilov, **(Sofia University)**;
Manuel Meyer, Igor Moskalenko, Nicola Omodei, Elena Orlando, Troy Porter, Giacomo Vianello, **(Stanford University)**;
Tim Linden, **(Stockholm University)**;
John Beacom, **(The Ohio State University)**;
S. Kaufmann, **(Universidad Autonoma de Chiapas)**;
Miguel A. Sanchez-Conde, Juan Abel Barrio, Alberto Dominguez, Marcos Lopez, Daniel Morcuende, **(Universidad Complutense de Madrid)**;
Sonia Anton, **(Universidade de Aveiro)**;
Rui Curado da Silva, **(Universidade de Coimbra)**;
Stephan Zimmer, **(Universitaet Innsbruck)**;
Martin Pohl, **(Universitaet Potsdam)**;
Sara Buson, **(Universitaet Wurzburg Lehrstuhl fur Astronomie)**;
Margarita Hernanz, Marc Riba, **(Universitat de Barcelona)**;
Enrico Bozzo, Roland Walter, **(Universite de Geneve)**;
Michael De Becker, **(Universite de Liege)**;
Inga Stumke, **(Universitetet i Bergen)**;
Silvia Zane, **(University College London)**;
Rodrigo Nemmen, **(Universidade de São Paulo)**;
Michael Briggs, **(University of Alabama Huntsville)**;
John Tomsick, Andreas Zoglauer, **(University of California Berkeley)**;
Steven Boggs, **(University of California San Diego)**;
Robert Johnson, David Williams, **(University of California Santa Cruz)**;
Jamie Holder, **(University of Delaware)**;
Pablo Saz Parkinson, **(University of Hong Kong)**;
Brian Fields, Xilu Wang, **(University of Illinois)**;
Markos Georganopoulos, Eileen Meyer, **(University of Maryland Baltimore County)**;
Peter Shawhan, **(University of Maryland College Park)**;
Bing Zhang, **(University of Nevada Las Vegas)**;
Fabian Kislat, Marc McConnell, Chanda Prescod-Weinstein, **(University of New Hampshire)**;
Jack Hewitt, **(University of North Florida)**;
Eugenio Bottacini, Michele Doro, Luca Foffano, **(University of Padova)**;
Denis Bastieri, Alessandro De Angelis, Elisa Prandini, Riccardo Rando, Luca Baldini, Barbara Patricelli, **(University of Pisa** & **INFN)**;
Francesco Longo, **(University of Trieste** & **INFN)**;
Stefano Ansoldi, **(University of Udine)**;

Wlodek Bednarek, **(Uniwersytet Lodzki)**;
Jim Buckley, Wenlei Chen, Henric Krawczynsiki, **(Washington University in St. Louis)**;
Harsha Blumer, **(West Virginia University)**;
Paolo Coppi, **(Yale University)**;

I Executive Summary

The All-sky Medium Energy Gamma-ray Observatory (AMEGO) is a probe class mission that will provide ground-breaking new capabilities for multimessenger astrophysics - identifying and studying astrophysical objects that produce gravitational waves and neutrinos. AMEGO also has compelling science drivers in astrophysical jets, compact objects, dark matter and nuclear line spectroscopy (**Figure 1**). AMEGO will cover the energy range from 200 keV to over 10 GeV, with more than an order of magnitude improvement in sensitivity relative to previous missions. The instrument performance characteristics are summarized in **Table 1**.

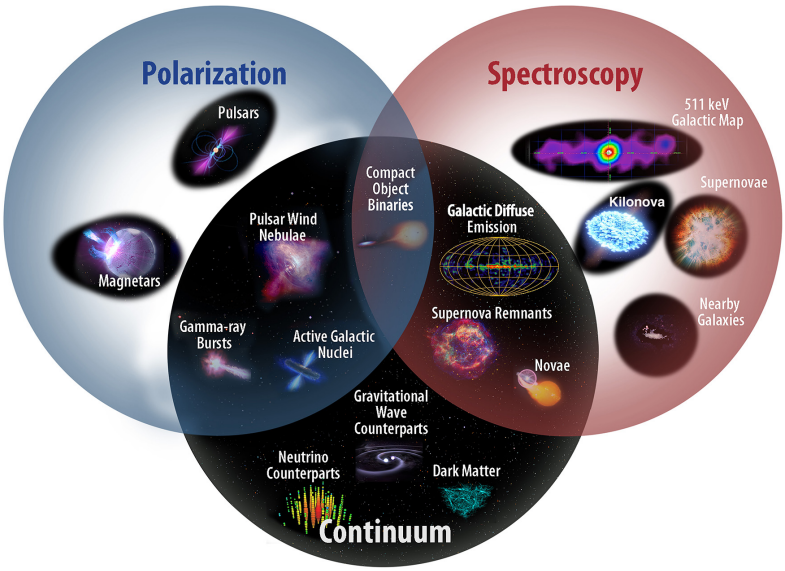

Figure 1: AMEGO will provide breakthrough capabilities in three areas of MeV astrophysics: a wide field of view and broad energy range will provide outstanding capability in time-domain and multimessenger astrophysics including excellent synergies with observations at other wavelengths; polarization capability will uniquely probe conditions and processes in astrophysical jets and in the magnetospheres and winds of compact objects; and nuclear line spectroscopy will bring new insight into element formation in dynamic environments.

Ground-Breaking Capabilities: Developments in detector technology since the last major mission in medium energy gamma-ray astrophysics enable a transformative probe class mission.

Community and partnerships: The AMEGO team is an international group of 200 scientists at 80 institutions. We have extensive experience designing, building, and operating gamma-ray telescopes. The team is supported by a broad community of observers and theorists with extensive experience exploiting gamma-ray observations.

Mature Technology: The technologies used in AMEGO are mature, and we have developed and tested key hardware and analysis tools with support from agencies in the US and Europe. The AMEGO subsystems and spacecraft have undergone preliminary engineering and costing studies that show that this mission is tenable within the probe class cost envelope.

Table 1: AMEGO's design has been optimized for excellent flux sensitivity, broad energy range, and large field of view.

Energy Range	200 keV to >5 GeV
Angular Resolution per Photon	2.5° (1 MeV), 2° (100 MeV), 1° (1 GeV)
Energy Resolution (FWHM/E)	1% (1 MeV), ~10% (1 GeV)
Field of View	2.5 sr (20% of the sky)
Line Sensitivity	1×10^{-6} ph cm^{-2} s^{-1} for the 1.8 MeV ^{26}Al line in 5 years
Polarization Sensitivity	<20% MDP for a source 1% the Crab flux, observed for 10^6 s
Sensitivity (MeV s^{-1} cm^{-2})	2×10^{-6} (1 MeV), 1×10^{-6} (100 MeV) in 5 years

II Science Overview

II.1 Science Objectives and Measurement Requirements

Briefly describe the scientific objectives and the most important measurements required to fulfill these objectives. Feel free to refer to science white papers or references from the literature.

AMEGO will play a critical role in the burgeoning area of multimessenger astrophysics [1]. Gamma-ray observations have played a key role in the three directions of multimessenger astrophysics: neutrinos and gamma-ray lines from SN1987A, a gamma-ray burst (GRB) and gravitational waves (GWs) from GW 170817, and high-energy neutrinos and a gamma-ray flare from the active galaxy TXS 0506+056. AMEGO's three scientific objectives tie directly to each of these.

The enormous discovery space for AMEGO achievable in the context of a probe-class mission flow directly from the fact that the medium-energy gamma-ray range (∼200 keV – ∼100 MeV) is a poorly explored part of the electromagnetic spectrum. Observations from the hard X-ray and high-energy gamma-ray bands that bracket the AMEGO range, together with the emergence of multimessenger astrophysics, provide assurance that AMEGO will pay off with major gains in our understanding of the extreme universe.

AMEGO's three scientific objectives focus on our understanding of sources known to produce non-photon messengers. These define the requirements for AMEGO's single instrument:

1. **Understand the physical processes in the extreme conditions around compact objects involved in gravitational wave events and other energetic phenomena** [2–6]. Because these are transient phenomena coming from random directions, the requirements are for good sensitivity (to collect enough photons), good energy resolution (to measure spectral features), sufficient angular resolution (to localize the transients), and large field of view (to detect enough events).
2. **Resolve the processes of element formation in extreme environments such as kilonovae and supernovae** [7, 8]. The gamma-ray line spectroscopy needed for these measurements requires good line resolution, high sensitivity, and effective rejection of background.
3. **Decipher the operating processes of jets in extreme environments such as gamma-ray bursts and active galactic nuclei** [9–14]. Multiwavelength/multimessenger time-domain astrophysics is the key to these observations, calling for a large field of view, good sensitivity, and rapid response to events. Polarization measurement capability adds an important diagnostic tool.

These qualitative requirements have been quantified through extrapolations from observations at other wavelengths and by simulations based on theory. These calculations were detailed in white papers submitted to the decadal survey: **https://asd.gsfc.nasa.gov/amego/science.html**. The requirements are largely defined by comparison to previous instruments operating in the medium-energy gamma-ray range:

- Continuum sensitivity a factor of 20 better than COMPTEL on the *Compton Gamma Ray Observatory*.
- Line sensitivity a factor of 10 better than *INTEGRAL*-SPI.
- Polarization sensitivity a factor of 5 better than *INTEGRAL*.
- Angular resolution a factor of 2 better than *Fermi* Large Area Telescope (LAT) at 100 MeV.
- Detection volume for gamma-ray bursts a factor of 25 greater than *Fermi* Gamma-ray Burst Monitor (GBM).

Beyond its three scientific objectives, AMEGO can be used as a general purpose observatory and address many additional science topics, as discussed in Astro2020 White Papers [15, 16].

II.2 Most Demanding Objectives

Of the objectives, which are the most demanding? Why?

Of the three science objectives, the third has aspects that are the most demanding, for two reasons:

- Jets from gamma-ray bursts and active galactic nuclei have been studied extensively, but they are complex phenomena and models are not well constrained even with the extensive resources already available.
- The AMEGO capability that is most likely to provide new insight is its ability to measure polarization and its energy and temporal dependen-

cies, but this is a challenging measurement in the AMEGO energy range.

Nevertheless, important multimessenger studies - finding and measuring timing and spectral properties of jets associated with gravitational wave events and high-energy neutrinos - are straightforward. Emerging capabilities in gravitational wave detectors and upgraded neutrino observatories combined with AMEGO's gamma-ray spectral, temporal and polarization observations will revolutionize this field.

II.3 Technical Requirements

Present the highest-level technical requirements (e.g. spatial and spectral resolution, sensitivity, timing accuracy) and their relation to the science objectives.

Specific values for the required performance parameters are given in the Science Traceability Matrix (STM), which relates these requirements back to the scientific objectives. The STM is shown in **Table 3**. The instrument performance characteristics are summarized in **Table 1**.

II.4 Performance Requirements

For each performance requirement, present as quantitatively as possible the sensitivity of your science goals to achieving the requirement. For example, if you fail to meet a key requirement, what would be the impact be on achieving the science objectives?

We have divided the measurements of our sensitivity into three broad areas based on the science requirements: continuum source sensitivity, narrow line sensitivity, and polarization sensitivity.

The sensitivity of AMEGO has been predicted through detailed simulations of the angular resolution, energy resolution, effective area, and background rates, as described in **Section III.1.1**. Using these results, we have calculated the AMEGO continuum source sensitivity shown in **Figure 2**. This is particularly important for detection of non-thermal emission from physical processes in the extreme conditions around compact objects. The AMEGO narrow-line sensitivity, which is a measure of the detectability of a source with gamma-ray line emission, is shown in **Figure 3**. The calculation takes into account the energy resolution of the instrument; therefore, good energy resolution is important for studying element formation in our Galaxy.

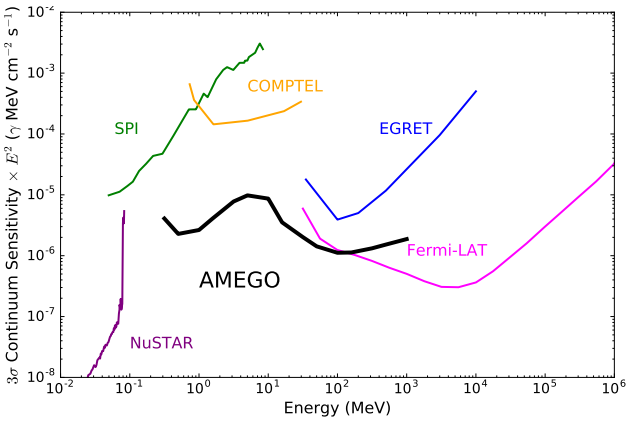

Figure 2: The simulated AMEGO 3σ on-axis point source continuum sensitivity. We assumed a 5-year mission or an exposure of 5 years with a 20% observation efficiency (due to field of view and SAA). For comparison, we show the sensitivity for the *Fermi*-LAT [17], which assumes the same incidence angle and efficiency for a 5 year mission. Two week sensitivities are shown for COMPTEL [18] and EGRET [19], which represent their typical exposure on any point on the sky, assuming a 40% efficiency. If we were to compare AMEGO with a 2 week exposure it would still have a sensitivity 10× better than COMPTEL. *NuSTAR* [20] and SPI [21] both assume an exposure of 10^6 s.

Table 2: Minimum Detectable Polarization for 1 Ms observations.

Flux of Target	AMEGO	INTEGRAL
Crab	<1%	~20%
100 mCrab	4%	
10 mCrab	30%	

Compton telescopes are inherently sensitive to polarization, and the AMEGO minimum detectable polarization (MDP) is shown in **Table 2**. Gamma-ray polarization measurements are a unique tool to understand acceleration mechanisms and the composition of jets from extreme objects.

There are no sharp changes in the AMEGO science performance parameters (sensitivity, field of view, angular resolution, energy resolution, polarization response, effective area, and sensitivity) with gradual degradation of subsystem performance.

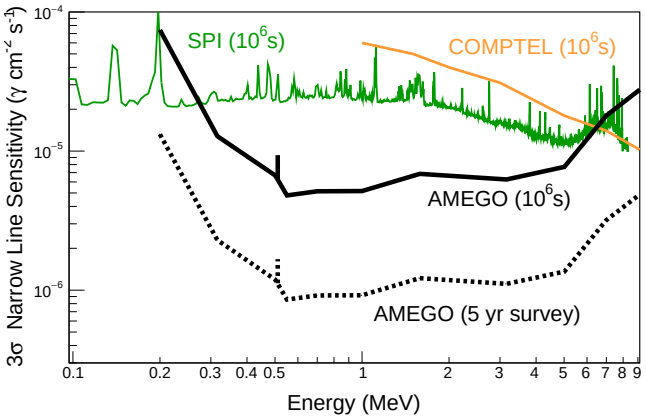

Figure 3: The narrow-line sensitivity for AMEGO from 200 keV to 9 MeV. AMEGO is an order of magnitude more sensitive at 1 MeV than *INTEGRAL*/SPI and COMPTEL. The 5 year survey sensitivity assumes a 30% observation efficiency. This includes both tracked and untracked Compton events. The slight reduction of the sensitivity at 511 keV is due to the large background contribution at that energy.

Table 3: Science Traceability Matrix

Science Goals	Science Objectives	Science Measurement Requirements		Instrument Requirements		Projected Performance	Mission Requirements	
		Physical Parameters	Observables	Parameter	Requirement		Parameter	Requirement
Understand the physical processes in the extreme conditions around compact objects involved in gravitational wave events and other energetic phenomena	What can neutron star mergers tell us about fundamental properties of gravity and spacetime?	Speed of gravity Weak Equivalence principle Lorentz Invariance Gravitational parity	Short duration GRB prompt emission in coincidence with gravitational wave detections	Absolute timing Field of view	<10 μs >2 Steradians	<3 μs >2.5 Steradians	Mission duration Orbit	5 years LEO: <10 deg inclination, 500-650 km altitude
	How often and how do neutron star mergers and collapsars produce successful relativistic jets, and what is the nature of those jets?	Ultrarelativistic particle acceleration Jet structure and role of viewing geometry Emission mechanisms Environment NS Equation of State	Relative time between the GW merger signal and the onset of the GRB. Gamma-ray observations of GRB prompt and afterglow emission, including polarization. Rapid localization to enable follow-up observations for multi-wavelength studies	Minimum Detectable Polarization Localization accuracy Continuum sensitivity Energy Range	<30% for a GRB with fluence of 8×10^{-6} erg cm^{-2} (300-3000 keV) <5 deg radius <5×10^{-6} erg cm^{-2} s^{-1} (1 MeV, 2 sec) 300 keV - 1 GeV	<20% for a GRB with fluence of 8×10^{-6} erg cm^{-2} (300-3000 keV) <1 deg radius <1×10^{-6} erg cm^{-2} s^{-1} (1 MeV, 2 sec) 200 keV - >5 GeV	Observing modes	all-sky survey mode inertial pointing mode
	What determines the diverse observed characteristics of different classes of neutron stars and their winds?	Emission mechanisms Environments Termination shocks Fundamental QED	Pulsar and magnetar broadband energy spectra, pulse-phase light curves, and polarization, including during variable states	Energy range Absolute timing Minimum Detectable Polarization	300 keV - 1 GeV <10 μs <30% for 10^{-10} erg cm^{-2} s^{-1} (300 keV, 2 yrs)	200 keV - >5 GeV <3 μs 5% for 10^{-10} erg cm^{-2} s^{-1} (300 keV, 2 yrs)	Sky survey uniformity Science data rate (orbit averaged)	>80% of sky at 5×10^{-5} γ MeV cm^{-2} s^{-1} (1 day) 5 Mbps
Resolve the processes of element formation in extreme environments, such as kilonovae and supernovae	What is the origin of heavy elements?	Nuclear yield of r-process elements in nearby KNe Source evolution of NS mergers and collapsars	Direct gamma-ray signal from nuclear transitions in KNe Redshift distribution of short and long GRBs	Continuum sensitivity Field of view	<5×10^{-6} γ MeV cm^{-2} s^{-1} (1 MeV) >2 steradians	<3×10^{-6} γ MeV cm^{-2} s^{-1} (1 MeV) >2.5 steradians	Pointing knowledge	30 arcsec
	What are the explosion mechanisms and progenitors of core collapse and Type Ia supernovae?	Distribution of ejecta SN explosion models Chemical composition of the progenitor star	Early monitoring ^{56}Ni gamma-ray line light curves of SN Type Ia Flux measurements of ^{44}Ti from young core-collapse SN remnants All-sky map of diffuse emission from ^{26}Al and ^{60}Fe Core-collapse SN with MeV neutrinos	Energy resolution Narrow line sensitivity (^{26}Al) Narrow line sensitivity (511 keV)	<2% FWHM (1 MeV) $<10^{-5}$ ph cm^{-2} s^{-1} (1.8 MeV, 10^6 s) $<4\times10^{-6}$ ph cm^{-2} s^{-1} (5 years)	1% FWHM (1 MeV) 5×10^{-6} ph cm^{-2} s^{-1} (1 MeV, 10^6 s) 2×10^{-6} ph cm^{-2} s^{-1} (5 years)	Pointing accuracy Absolute timing accuracy	10 deg <10 μs
	What are the sources of Galactic positrons?	Galactic distribution of positron annihilation Positron propagation limits Positron source contributions	All-sky diffuse image of 511 keV and ortho-positronium continuum Comparison with ^{26}Al in star forming regions Continuum spectrum >511 keV	Field of view Angular Res. (511 keV) Continuum sensitivity	>2 steradians <5 deg (FWHM) <5×10^{-6} γ MeV cm^{-2} s^{-1} (1 MeV)	2.5 steradians 3 deg (FWHM) <3×10^{-6} γ MeV cm^{-2} s^{-1} (1 MeV)	Data Latency: Transient Alerts Survey Data	30 s 24 hrs
Decipher the operating processes of jets in extreme environments such as gamma-ray bursts and active galactic nuclei	What are the particle acceleration mechanisms that drive jet composition and energy transport?	Distinguish leptonic/ hadronic emission models Emission mechanism Particle acceleration Neutrino production	Spectral and temporal evolution of GRB prompt and afterglow emission Long-term monitoring of blazars in coincidence with high-energy neutrino detections Polarization	Minimum Detectable Polarization Field of View	<20% for a 100 mCrab source in 10^6 sec >2 steradians	4% for a 100 mCrab source in 10^6 sec 2.5 steradians		
	What astrophysical sources produce high-energy neutrinos?		Broadband gamma-ray SEDs and temporal variability of MeV-peak blazars	Energy range	300 keV - 1 GeV	200 keV - >5 GeV		

III Technical Implementation

III.1 Instrumentation

III.1.1 Science Instrumentation

Describe the proposed science instrumentation, and briefly state the rationale for its selection. Discuss the specifics of each instrument (Inst 1, Inst 2 etc) and how the instruments are used together.

To achieve the scientific goals in **Section II**, we require an instrument capable of imaging gamma rays over a wide field-of-view and a broad energy range. This energy range is uniquely challenging, because of how photons interact with detector materials: both via Compton scattering at lower energies ($\lesssim$ 10 MeV) and via pair production at higher energies ($\gtrsim$ 10 MeV). Thick detectors are needed to fully contain these interactions, and a precise measure of the tracks through the instrument volume are needed to reconstruct the original gamma-ray direction. Furthermore, the MeV regime is background dominated; therefore, techniques to reduce the background contribution, such as decreasing passive material near the detector, are necessary.

These goals can be accomplished with an instrument that generally consists of a "tracker," which allows for a reconstruction of charged particle tracks, and a calorimeter to measure the energy of incident gamma rays. As shown in **Figure 4**, the AMEGO tracker serves a dual purpose: it acts as a Compton-scattering element for low-energy gamma rays or pair-conversion material for high-energy gamma rays. Ionizing charged particles, either a Compton-scattered electron or the electron and positron pair-conversion products, deposit energy and allow for the direction to be tracked. The AMEGO design includes two calorimeters. The first is a low-energy precision calorimeter optimized to measure the Compton-scattered photon with excellent energy resolution and position resolution. This calorimeter provides enhanced line sensitivity, good angular resolution in the Compton regime, and polarization capabilities up to a few MeV. To extend the sensitivity of AMEGO into the pair-conversion regime, we require a second calorimeter to contain high-energy events. This calorimeter is designed based on the calorimeter in *Fermi*-LAT [17]. Finally in this space environment, the number of cosmic-ray background events outnumbers gamma rays by orders of magnitude. To mitigate the effect of these events, we require an Anti-Coincidence Detector (ACD). This subsystem is the first-level defense against this background, so it must cover the top and four sides of the tracker.

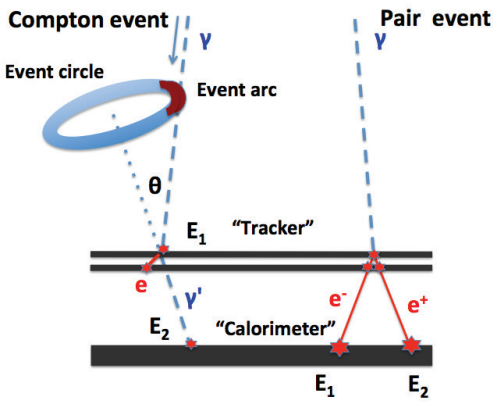

Figure 4: AMEGO detects gamma rays through both pair production and Compton scattering. In a Compton event, an incident gamma ray scatters by an angle θ in the tracker, transferring energy to an electron, and is then absorbed in the calorimeter. With this information we derive an 'event circle' to describe the arrival direction of the original photon. If the direction of the Compton-scattered electron is measured, the circle is reduced to an 'event arc'. In a pair event, an incident photon converts to an electron-positron pair in the tracker, allowing derivation of the original photon direction. The pair ultimately produces an electromagnetic shower in the calorimeter, the directions of which permit derivation of the photon energy.

The AMEGO instrument concept with all four detector subsystems is shown in **Figure 5**. For ease of construction, the three instrument subsystems contained inside the ACD (Tracker, High and Low Energy Calorimeters) are divided into four identical towers illustrated in **Figure 6**, where the electronic readout is positioned at the edges to minimize passive material in the active area. The detector subsystems are described in further detail below.

Tracker: To provide sufficient probability of a gamma-ray interaction in the tracker while minimizing the effects of multiple-scattering, the AMEGO tracker consists of 60 layers of 500 μm thick silicon detectors (**Figure 7**). Position sensitivity within each tracker layer is needed to measure the Compton-scattered electron. This is achieved through the use of double-sided silicon detectors (DSSDs), where orthogonal strips on each side of

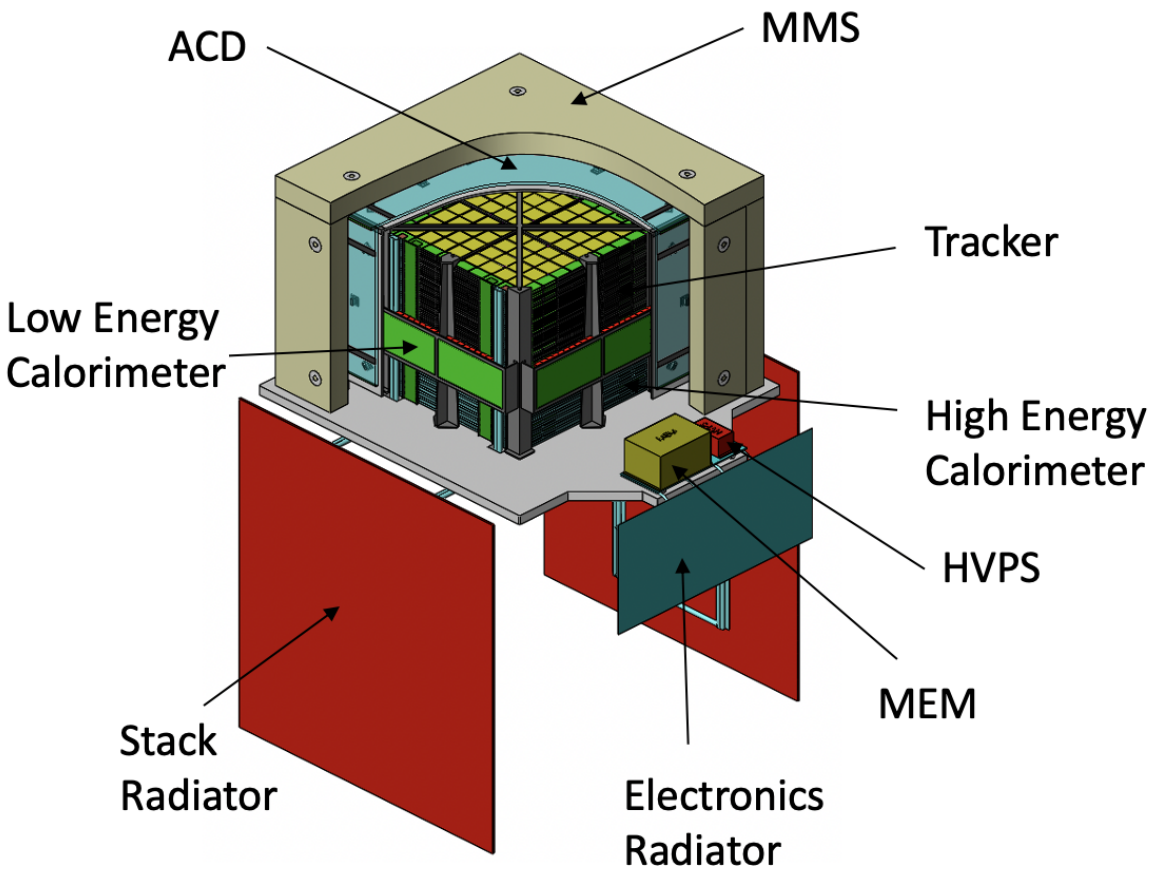

Figure 5: A mechanical CAD model of AMEGO highlights the four subsystems with the micrometeoroid shield (MMS) and Anti-Coincidence Detector (ACD) cutaway to expose the tower structure. The full instrument measures 1.6×1.6×1.2m. The Double-Sided Silicon Detectors (DSSDs displayed in yellow) are stacked in 60 identical layers. The Low-Energy Calorimeter modules sit beneath and cover the outer sides of the lower layers of the tracker modules. The High-Energy Calorimeter modules consist of hodoscopic layers of crystal logs at the base of the instrument. The electronics readouts are illustrated in green. The four towers sit within top and side panels of the ACD. The MMS and thermal blanket cover the top and sides of the instrument. For completeness, the instrument includes a Main Electronics Module (MEM), a high voltage power supply (HVPS) and radiators.

the detector are used to determine the position of the interaction. The optimal DSSDs strip geometry, driven by the required position resolution and the expected uncertainty due to multiple-scattering, is 500 μm strip pitch yielding 190 channels per side per wafer. Each layer is a 4×4 array of DSSDs, each 9.5 cm square. The strips on neighboring detectors are daisy-chained together through wire bonds to minimize the number of electronic channels and the amount of passive material. The angular resolution in the pair regime scales with the separation between tracker layers; therefore, we have chosen a 1.0 cm separation.

An accurate measurement of the energy deposited in the silicon tracker is necessary in the Compton regime; therefore, an analog readout of the DSSDs is required. The signal processing and analog-digital conversion for each strip is done in readout ASICs on the edge of the layer. Additionally, we require a minimal amount of passive material in the active DSSD area, as passive material will absorb low-energy electrons and scattered photons and thus render these events unusable. There is a minimized mechanical structure composed of composite materials supporting the DSSDs and readout (described further below).

Low-Energy Calorimeter: To enhance the low-energy response of AMEGO, the Low-Energy Calorimeter provides precise measurements of the energy and position of the Compton-scattered pho-

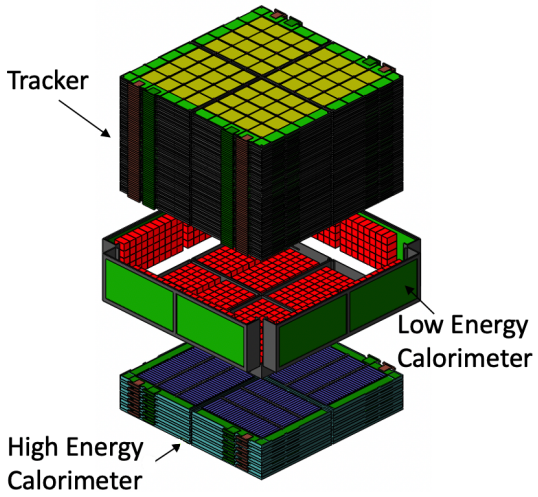

Figure 6: A mechanical CAD model of the four AMEGO towers highlighting the three inner subsystems that make up the towers. The Tracker is stacked in 60 layers. The Low-Energy Calorimeter modules, made of Cadmium Zinc Telluride (CZT) bars, sit both beneath and cover the outer sides of the lower layers of the tracker modules. The High-Energy Calorimeter modules, made of Cesium Iodide doped with Thallium CsI(Tl), consist of hodoscopic layers of crystal logs at the base of the instrument. The four towers sit within top and side panels of the ACD, shown in **Figure 5**.

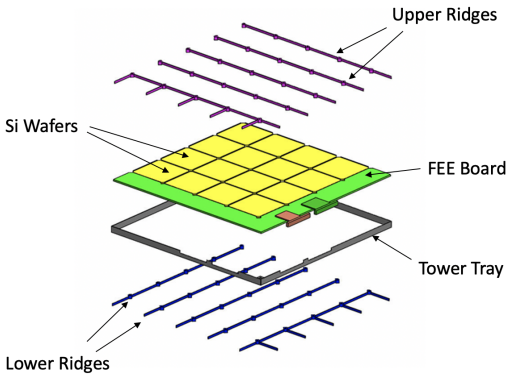

Figure 7: A challenge of this energy regime is that gamma rays are particularly affected by passive material within the active detector volume. The AMEGO tracker design minimizes the passive material within the active Si wafer area array by minimizing a ridge structure (both above and below the tower tray for support) made of low-Z composite materials. An exploded CAD view of this ridge structure, with the Si wafers, front end electronics (FEE) board and tower tray is displayed.

ton (**Figure 8**). The Low-Energy Calorimeter is designed to surround the Tracker. The calorimeter covers approximately the bottom third of the tracker to maximize the detectable Compton scatter angle while maintaining a large field of view.

The design uses 8 mm × 8 mm × 40 mm Cadmium Zinc Telluride (CZT) bars with a virtual Frisch-grid readout [22]. The thickness of these detectors is maximized since the interaction depth of gamma rays is ∼10 g/cm^2 at 1 MeV; this calorimeter yields approximately three radiation lengths. With only 6 channels per bar, this readout gives excellent energy resolution <1% FWHM at 662 keV, and position resolution <1 mm in all 3 dimensions [23]. Compared with other CZT detector configurations, such as pixelated electrodes, the virtual Frisch-grid detector can use CZT of lesser quality, has fewer electronic channels, uses a lower bias voltage, and are readily integrated into a large-area arrays [24].

The calorimeter is built to be modular for ease of construction. The base unit is a 4 × 4 array of CZT bars mounted in a carrier fabricated of printed circuit board (PCB) to provide structural support as well as the electrical connections to the detector electrodes. This module of 16 bars, which aggregates to 3.7 cm × 3.7 cm × 6 cm, has a single readout ASIC. These modules are mounted to a motherboard consisting of 5×10 CZT arrays to form a full CZT module consisting of 800 bars. Two arrays are placed below the active area of the tracker and two arrays are rotated to cover the lower sides of the tracker. These side CZT calorimeter arrays increase the polarization performance as the sensitivity to polarization is larger for larger scatter angles. Altogether, there are 3040 CZT bars (4 arrays) per tower.

High-Energy Calorimeter: We have designed a calorimeter optimized for high-energy gamma rays based on the design of the *Fermi*-LAT [17]. The AMEGO High-Energy Calorimeter uses Thallium-doped Cesium Iodide (CsI(Tl)) crystal bars with dramatically improved performance by collecting the scintillation light with silicon photomultipliers (SiPMs) (**Figure 9**). SiPMs provide further advantages in being a fraction of the size and mass of photomultiplier tubes (PMTs), and they operate at a low bias voltage to achieve a similar gain. To fill the area beneath the Tracker, each calorimeter module consists of 6 layers of 26 CsI(Tl) bars, each 1.5 cm × 1.5 cm × 38 cm, arranged hodoscopically. This calorimeter provides an additional five

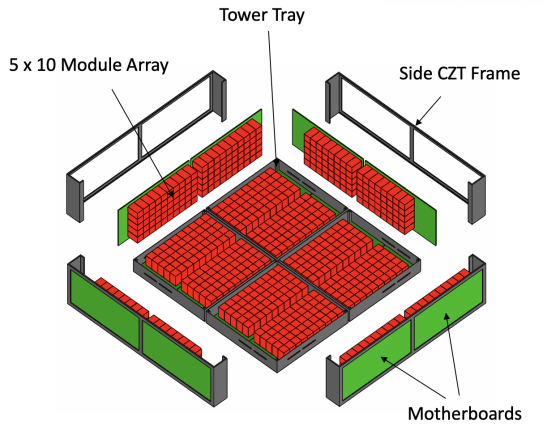

Figure 8: The Low-Energy Calorimeter serves a unique purpose: supplying both excellent position and energy resolution for events that interact via Compton scattering in the Cadmium Zinc Telluride (CZT) bars. The side arrays detect photons scattered at large Compton scattering angles which is particularly important at low energies. The tower arrays are all identical for ease of construction. The side frames and tower trays are made of composite material. An exploded CAD view of the frame, trays, arrays, with the CZT modules (in red), and motherboards is displayed.

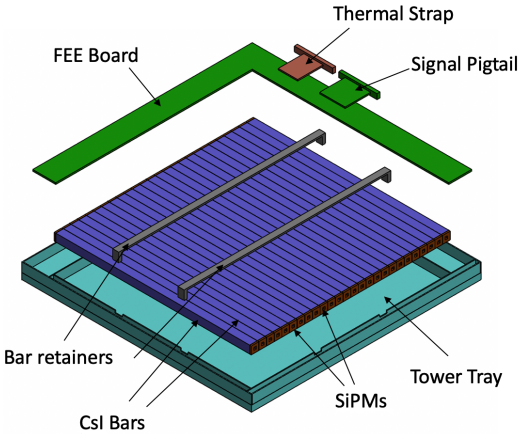

Figure 9: The High-Energy Calorimeter design is inspired by the design of the *Fermi*-LAT calorimeter. It extends the high-energy Capabilities of AMEGO allowing for overlap in energy coverage with the LAT. Layers of CsI(Tl) bars are arranged hodoscopically allowing 3D position resolution of the showers complementing the other instrument subsystems. Detector electronics are located on the edges of the bars, which are read out via a 2×2 array of SiPMs. The bars are supported by a composite tower tray. An exploded CAD view of a single layer with a tower tray and front end electronics (FEE) board, with the CsI(Tl) bars (in blue) and SiPMs is shown.

radiation lengths and extends the sensitivity above ∼100 MeV.

The CsI(Tl) bars are wrapped in a reflective material to give high light collection efficiency and the scintillation light is read out by a SiPM bonded at each end. By comparing the relative amplitude of the SiPM readout on each end, an internal position resolution of 1 cm σ at 1 MeV is achieved [25]. Matching energy deposits in the calorimeter with events recorded in the tracker allows for a better recognition of background cosmic-ray deposition and thus increases the sensitivity at high energies.

Anti-Coincidence Detector: To cleanly distinguish the largest background contaminant (cosmic rays) from the photons of interest, AMEGO utilizes a plastic scintillator anti-coincidence detector (ACD), which surrounds the tracker and Low-Energy Calorimeter (**Figure 10**). Any cosmic ray that passes through the ACD will result in a response and thus the event can be identified as a charged particle event. The AMEGO ACD design is based on the ACD built for the *Fermi*-LAT and uses the same plastic scintillator as the detector material [26].

The AMEGO ACD consists of five panels that are 134 cm × 87 cm × 1.5 cm with wavelength shifting (WLS) strips and a SiPM readout. WLS strips are inserted in grooves in each panel edge and viewed by two SiPMs, allowing more uniform light collection than with SiPMs alone. The use of SiPMs for the readout has the advantage of low mass and low bias voltage while still maintaining the same performance as a traditional PMT.

Mechanical: The core principle of the mechanical design of the AMEGO instrument is that each subsystem is comprised of identical components for ease of construction and assembly. This also has the advantage of reducing the number of unique parts and assemblies thereby reducing the cost of fabrication and tooling. For the tracker and High-Energy Calorimeter subsystems, the component is the layer (illustrated in **Figure 7** and **Figure 9** respectively). For the Low-Energy Calorimeter, it is a the array. For the ACD, the component is the panel.

The structural design is driven by the requirement to support a large number of components while minimizing the structural interference within the active area of the detector. Metal structural elements are

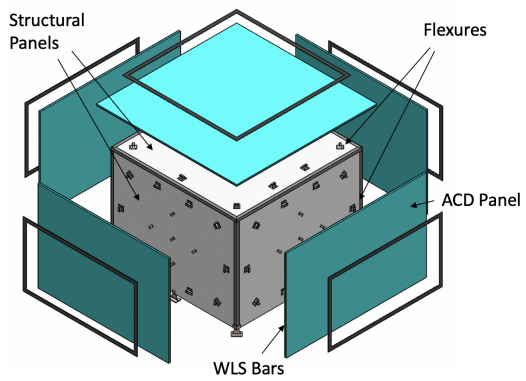

Figure 10: Cosmic rays are a dominant background and outnumber gamma rays by orders of magnitude in this energy range. The Anti-Coincidence Detector is the first line of defense against this background, providing a veto to charged particle interactions. The AMEGO ACD, made of five scintillating plastic panels and read out by SiPMs connected to wavelength shifting (WLS) bars, surrounds the tracker and side Low-Energy Calorimeter. It is based on a simplified version of the *Fermi*-LAT ACD which has successfully vetoed cosmic rays on orbit for more than a decade. An exploded CAD model is displayed with structural panels and fixtures.

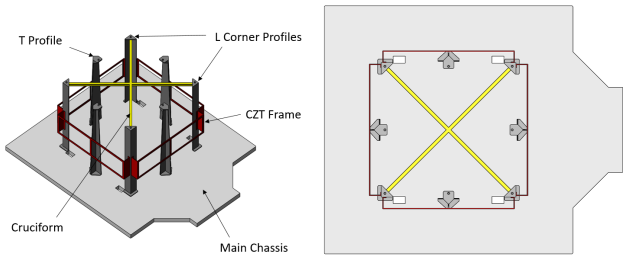

Figure 11: Top-level structure assembly is designed to minimize passive material near the sensitive detector components. The corner posts and frame structure are made of low-Z composite material to reduce activation within the instrument. A cruciform structure connects the corner posts to prevent the drumhead effect on the instrument stack. The assembly structure is mounted to the aluminium honey comb chassis which serves as the interface with the spacecraft.

not used within the instrument field of view, and all primary structural elements were designed using low-Z carbon composite materials, baselined to be M55J, to reduce activation.

The tracker tower is supported by a matrix frame and tray mounting frames all made of composite material. Individual layers are keyed using alignment pins, which provide rigidity and shear strength. In order to simplify integration, no interface screws will be added, and the layers will stack on top of each other with alignment pins. These pins will limit the relative displacement of adjacent trays in the XY plane. The resulting stack is very rigid. The stack is keyed to the spacecraft interface plate with shear pins and preloaded in the axial direction using posts that capture the instrument along its periphery, holding it down against the spacecraft interface plate. The posts also provide mounting for the CZT frame that holds the side CZT detectors, making all members work together against launch loads (see **Figure 11**).

In order to minimize the drumhead effect on the tracker layer stack, a cruciform is added to connect the corner posts with enough preload to prevent gapping in the launch environment. The main chassis is an aluminum honeycomb panel, serving as the interface with the spacecraft. Due to differences in the coefficient of thermal expansion between Al and composite, a composite honeycomb panel is an appropriate choice based on how the posts are mounted. The ACD panels are supported with a simple frame and panel structure. The scintillator material mounted to the ACD panels is a lightweight plastic material so the structure is self-supporting. Composite flexures mount the panel assembly to the chassis. The CZT arrays are mounted to a baseplate and will likely have interlocking top plates. The egg-crate structure of the modules supporting the bars combined with the interlocking upper panels and the integral lower panel creates a pseudo-isogrid assembly. Preliminary analysis indicates the structure required for the instrument design far exceeds the structural requirements imposed by expected loads. The structure, as a complete system, has gone through an analysis-based sizing process, based upon Finite Element Modeling of early concepts and its applicable launch loads (see **Figure 12**). Furthermore, at a lower assembly level, simplified calculations were done to predict that the individual silicon wafers and the CZT modules would not break under quasi-static loading and vibration.

Electrical: The AMEGO electronics system (**Figure 13**) consists of the MEM (Main Electronics Module), two HVPS (High Voltage Power Supplies), and tower components. The MEM converts the 28V power supply bus and distributes power to, controls, and collects data from the instrument tower subsystems. The tracker and two calorimeter tower subsys-

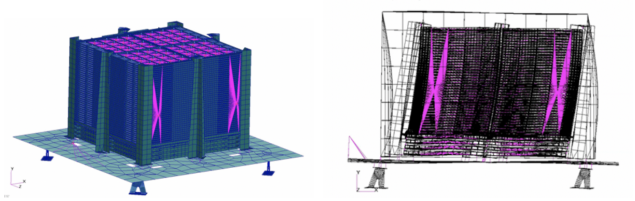

Figure 12: The structure, as a complete system, has gone through an analysis-based sizing process, based upon Finite Element Modeling of early concepts and its applicable launch loads. (Note: Vibrations shown on *right* are not to scale).

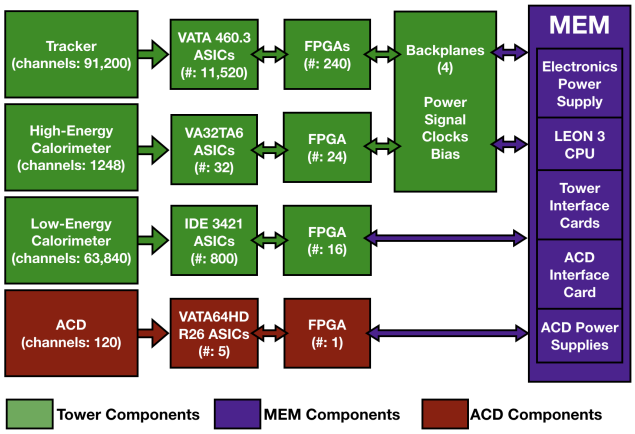

Figure 13: Each electrical subsystem interfaces with the MEM which provides power and data lines. The Tracker and High-Energy Calorimeter are connected via a backplane while the ACD and Low-Energy Calorimeter are connected via standard harnessing. Shown here are the major components of the electrical system highlighting the interfaces with the ASICs, FPGAs and MEM. The MEM interfaces to the spacecraft via SpaceWire and the spacecraft provides a standard 28 V line to power the instrument.

tems each have their own additional electronics and readout systems which relay relevant data upstream to the MEM for down-link.

A backplane is used to provide power distribution as well as digital communication from both the Tracker and High-Energy Calorimeter subsystems to the MEM. There is one backplane per tower, these can be seen on the left side of the instrument in **Figure 12**, where the signal pigtails on the FEE of each Tracker and High-Energy Calorimeter segment are shown in **Figure 7** and **9**. The communication and power distribution from the MEM to the Low-Energy (CZT) Calorimeter and ACD subsystems will use wiring harnesses. This combination of backplane and wiring harnesses will allow for easier test and integration while preserving the ability to achieve science objectives through proper placement.

Thermal: AMEGO features a passive thermal design (**Figure 14**) that utilizes common, high TRL components such as multi-layer insulation (MLI), radiators, heat pipes, isolators, and heat straps. Each tower stack of 60 trays and calorimeters is coupled to a dual-bore, ammonia heat pipe via numerous thermal straps. The straps transport the waste heat to the evaporator section of the heat pipe. The condenser end is well coupled to one of two 1.7 × 1.8 m radiators, coated with white paint on the space facing side and MLI on the spacecraft facing side. Two of the trackers are coupled to the "North" radiator and the other two trackers are coupled to the "South" radiator. The radiators are aluminum honeycomb sandwich panels with embedded heat pipes to improve the heat spreading efficiency. They were sized for 15% power growth above the expected dissipation of 950 W while maintaining the tracker interface temperatures below +20°C. A second thermal control system to reject the waste heat from the MEM and HVPS consists of 4 header, dual bore ammonia heat pipes that couple the electronics baseplate to a dedicated electronics radiator. The design of the mission allows for 360° of rotation around the boresight, which allows for the radiators to be kept nearly parallel to the solar vector, minimizing the solar heating on the radiators. Furthermore, the radiators are also kept nearly parallel to the nadir vector, minimizing the view of planetary IR emission on the radiators as well. The entire design is testable on the ground in the presence of gravity with the 4 tracker header pipes level, the tracker radiator spreader pipes in reflux mode, the electronics header pipes in reflux, and the electronics radiator spreader pipes level.

Evaluation of Instrument Performance: To estimate the performance of an MeV gamma-ray telescope, accurate instrument simulations are vital. It is essential to develop a complete mass model of the active and passive material and simulate gamma-ray interactions within the instrument volume. A detailed description of the backgrounds contributions, both externally and internally via activation within the detector material, are critical.

We have carried out detailed simulations, event reconstructions, and performance estimates of the

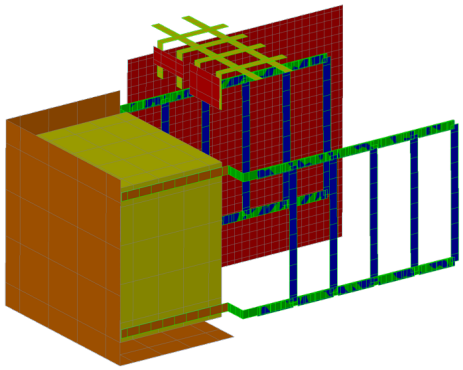

Figure 14: The design of the AMEGO Thermal Heat Pipe Network allows for full thermal testing on the ground in the orientation shown here.

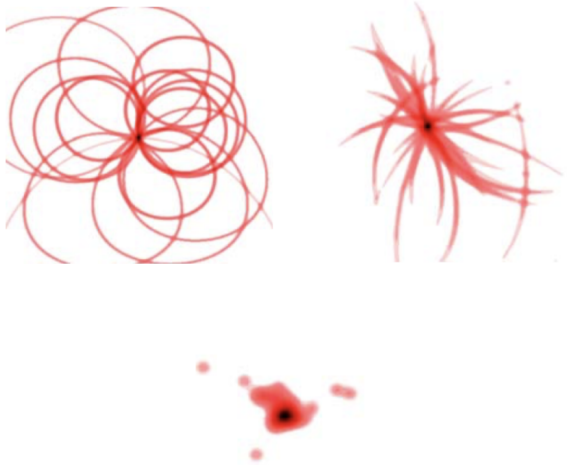

Figure 15: The backprojected image-space response for the three different AMEGO event types: untracked Compton events (upper left); tracked Compton events (upper right); pair events (bottom center) [30]. The advantage of tracked Compton events is better background rejection.

AMEGO instrument using the MEGAlib framework [27] which is based on ROOT [28] and Geant4 [29]. The AMEGO geometry and all of the simulation files used for this analysis can be found on GitHub[1].

We consider three different event classes, broadly defined in terms of the energy of the incident photon: untracked Compton events (untracked), tracked Compton events (tracked), and pair events. The distinction between tracked and untracked Compton events is whether or not the direction of the Compton-scattered election is measured. Each is optimized for different science cases. **Figure 15** illustrates a back-projection of ∼20 events showing the image-space response from individual photons for an AMEGO-type instrument.

At energies below ∼1 MeV, the Compton-scattered electron does not transit more than one tracker layer and therefore it cannot be easily tracked. As a result, the untracked event class will be important for transient science cases such as gamma-ray bursts that have strong emission $\lesssim$1 MeV and gamma-ray line astronomy, such as the decay of the SN products ^{56}Ni and ^{44}Ti. For sources that produce gamma-rays at higher energies (1–10 MeV) that require better background rejection, the tracked event class will likely be the standard event type used. For sources that produce photons above ∼10 MeV, the pair event class can be used in standard analyses.

We have performed MEGAlib simulations to determine the angular and energy resolution of the AMEGO instrument for mono-energetic sources. The energy resolution is particularly important in the MeV regime where sources of gamma-line emission are prominent. The angular resolution not only affects the quality of images, but aids in reducing source confusion and enhancing the sensitivity. The angular resolution for Compton and pair telescopes are defined in slightly different ways:

- *Compton Events*: The angular resolution measurement (ARM) is the smallest angular distance between the known source location and the Compton event circle for each photon. The total ARM histogram from a sample of Compton events is the effective point spread function (PSF) of telescope. The FWHM of the ARM distribution defines the angular resolution of a Compton telescope.

- *Pair Events*: For pair events, the reconstruction of tracks provides a single direction. The PSF is the angular difference between the true and reconstructed photon direction. We characterize the resolution as the 68% containment of the PSF.

The existing MEGAlib reconstruction algorithms for tracked Compton events and pair events were originally developed for the MEGA prototype [31] and are not yet optimized for AMEGO. APRA funds

[1] https://github.com/ComPair

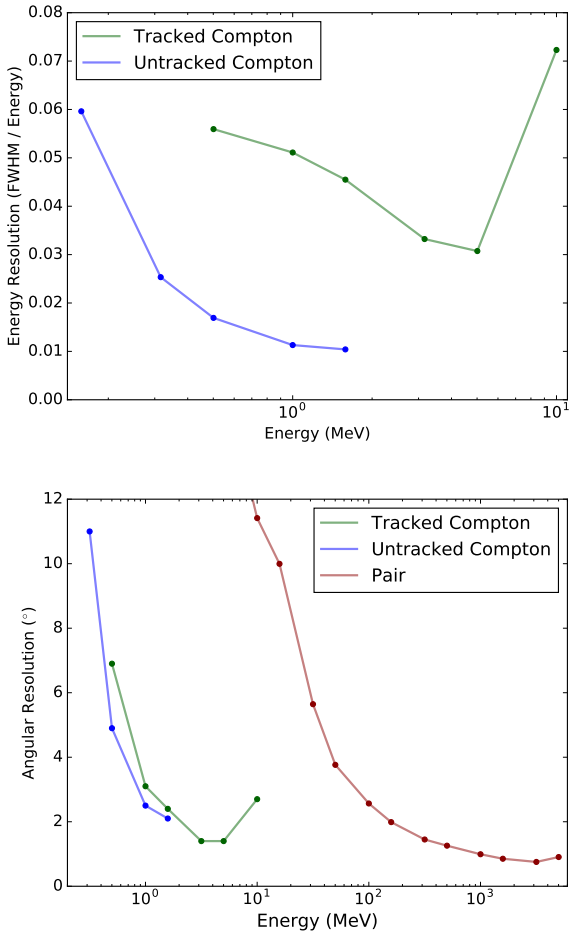

Figure 16: *Top:* The energy resolution as a function of energy, given as a percent in FWHM/Energy, is shown for Compton events. Untracked events have an energy resolution of ∼1% at 1 MeV. In the pair regime the energy resolution is ≲30%; this is not show here because it does not drive science requirement. *Bottom:* The angular resolution as a function of energy for the pair, tracked and untracked event classes. The best performance in the Compton regime is achieved at 1–5 MeV where the angular resolution is <2°. In the pair regime, the angular resolution is below 2° above 200 MeV.

were awarded to the head developer of MEGAlib who serves as the AMEGO ground processing and data analysis lead (PI: Zoglauer), to better and more efficiently implement reconstruction algorithms and event classification. These have not yet been implemented in our simulations, and therefore the performance estimates are conservative.

Figure 16 shows the energy resolution for Compton events and the angular resolution for all three event types across the energy range of the instrument. The simulations demonstrate that

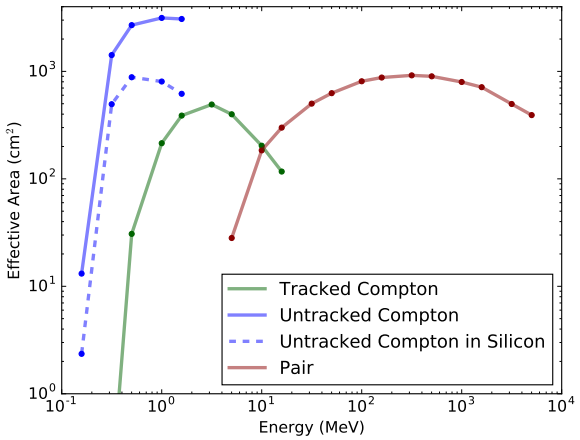

Figure 17: Effective Area ($A_{\rm eff}$) as a function of energy for on-axis sources. The effective area for untracked events is so large because this is the most probable type of interaction at low energies. The dashed blue curve is a subset of untracked Compton events which require the first interaction to be within the silicon tracker, where the solid blue curve allows for events that only interact in the Low-Energy CZT Calorimeter.

the AMEGO instrument achieves the angular and energy resolution required for each science case (**Table 3**). The energy resolution is particularly important for studying processes of element formation and the angular resolution plays an important role in the location accuracy of transient detections.

The effective area ($A_{\rm eff}$) is a measure of the efficiency of a telescope. It is defined as the area of an ideal absorber that detects an equivalent number of incident photons. The effective area can be found through simulations by:

$$A_{\rm eff} = \frac{N_{det}}{N_{start}} \times A_{\rm start} \qquad (1)$$

where $N_{\rm det}$ is the number of detected events, $N_{\rm start}$ is the number initial simulated photons, and $A_{\rm start}$ is the simulated area surrounding the mass model. To keep the performance estimates as general as possible, we have defined $N_{\rm det}$ to be the number of reconstructed events with open event selections. The simulated effective area is shown in **Figure 17** as a function of energy for each event class of AMEGO. For comparison, the effective area of COMPTEL reaches 40 cm^2 at 5 MeV.

In order to evaluate the polarization sensitivity of AMEGO, we performed a set of simulations with 100% linearly polarized photons. The amplitude of

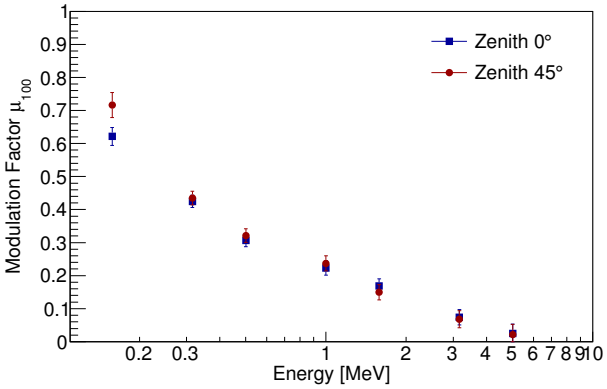

Figure 18: AMEGO is sensitive to polarization in the Compton regime. The modulation factor μ_{100}, shown here for AMEGO at two incident zenith angles, gives a measure of the observed modulation for a 100% polarized beam. AMEGO's polarization sensitivity is highest at a few hundred keV.

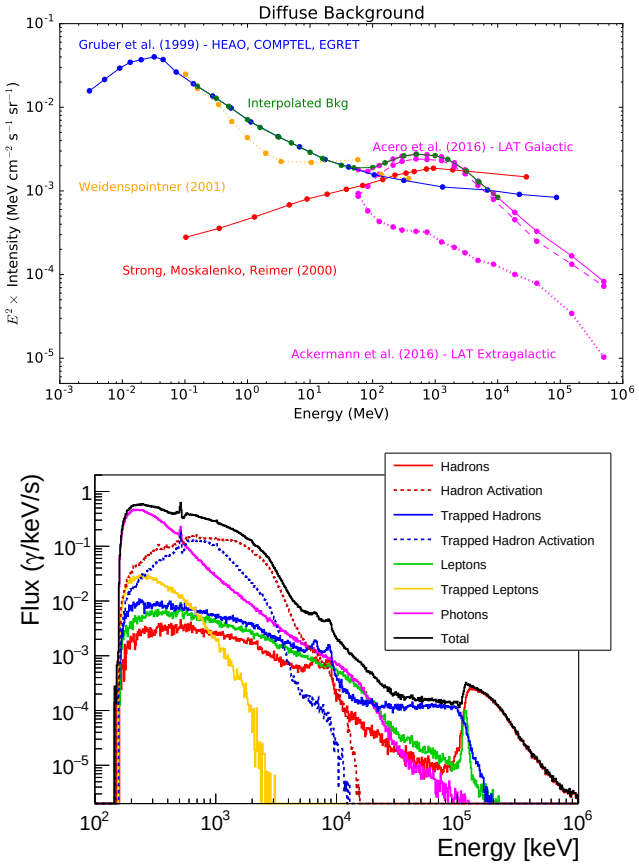

Figure 19: *Top* Modeled background components from 10 keV to 1 TeV. We have used the well-known background flux to determine the background in the pair regime, i.e. greater than 10 MeV. *Bottom* The simulated spectrum of fully reconstructed events for each background component from MEGAlib's *BackgroundGenerator* tool. These modeled components assume an orbit altitude of 600 km, inclination angle of 6°, and an average geomagnetic cutoff of 11.9 GV. We have used these spectra to determine the background rates below 10 MeV after the ACD veto.

the resulting azimuthal scattering-angle modulation gives the polarization signal. For a 100% polarized beam, this amplitude is called the modulation factor, μ_{100}, and is effectively the polarization signal strength inherent to the instrument. The AMEGO μ_{100} is shown in **Figure 18** as a function of energy for two different incident zenith angles. From μ_{100}, the minimum detectable polarization at the 99% confidence level can be determined for a specific observation:

$$\mathrm{MDP} = \frac{4.29}{\mu_{100}\, R_S}\sqrt{\frac{R_S + R_{BG}}{T_{\mathrm{obs}}}}, \qquad (2)$$

where R_S and R_{BG} are the signal and background event rate from a given source, respectively, and T_{obs} is the observation time. **Table 2** shows the calculated AMEGO MDP for observations at multiple source fluxes.

Background Simulations An accurate description of the background environment is necessary to predict the sensitivity of the instrument. We have separated the background treatment into two separate regimes: above 10 MeV we have used the well known backgrounds from *Fermi*-LAT and below 10 MeV we have performed detailed simulations of the background in MEGAlib which include gamma-ray, particle, and induced activation components.

A summary of the modeled background is shown in **Figure 19**. Measurements from HEAO, COMPTEL, EGRET [32], and *Fermi*-LAT [33, 34] are combined to describe the known cosmic background across the AMEGO energy range. Strong, Moskalenko, and Reimer [35] have modeled the diffuse gamma-ray continuum from cosmic rays, which is also included here. For energies $\gtrsim$10 MeV, the background is fairly well known from measurements from *Fermi*-LAT and we have estimated the AMEGO background flux from these models.

The backgrounds in the Compton regime ($\lesssim$10 MeV) are less understood and are often dominated by activation, therefore detailed simulations are necessary to determine the expected background rates. MEGAlib has a tool (*BackgroundGenerator*) which generates the spectral and spatial distribu-

tions for cosmic and albedo gamma-rays, protons, neutrons, alpha particles, electrons, and positrons, as well as trapped hadrons. We have assumed an orbit altitude of 600 km, inclination angle of 6°, and an average geomagnetic cutoff of 11.9 GV for these models. **Figure 19** ***bottom*** shows the resulting simulated spectra after reconstruction for 1 hour of observations for each of the modeled components. As can be seen in this figure, the dominant background source at ∼1 MeV is activation from hadronic particles.

III.1.2 Instrument Technical Maturity

Indicate the technical maturity level of the major elements and the specific instrument TRL of the proposed instrumentation (for each specific Inst 1, Inst 2 etc), along with the rationale for the assessment (i.e. examples of flight heritage, existence of breadboards, prototypes, mass and power comparisons to existing units, etc). For any instrument rated at a Technology Readiness Level (TRL) of 5 or less, please describe the rationale for the TRL rating, including the description of analysis or hardware development activities to date, and its associated technology maturation plan.

The philosophy behind the AMEGO design is heritage and experience. It relies heavily on the *Fermi*-LAT design and technical maturity from other high-energy missions.

An AMEGO prototype is also currently being supported by several funded APRAs: ComPair (PI: McEnery), CZT calorimeter (PI: Thompson) and CsI calorimeter (PI: Grove, PI: Woolf). As part of the APRA work, we have designed and are currently building small versions of each detector subsystem to validate the over-all design. We will test the functionality of the subsystems working together to reconstruct Compton and pair-conversion events in a beam test scheduled for summer 2020 and demonstrate functionality in a relevant environment via a balloon flight in fall 2021.

As AMEGO is divided into four instrument subsystems, the TRL for each is described in detail below.

Tracker: As discussed in **Sec. III.1.11**, all major components of the AMEGO tracker have flight heritage from missions including *Fermi*-LAT, AMS-02, Astro-H, PAMELA, and others.

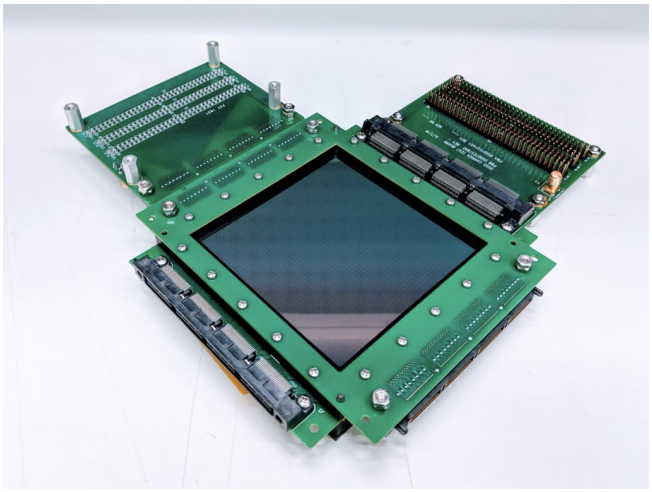

Figure 20: The AMEGO tracker prototype detector development is led by GSFC. The prototype consists of 10 layers of 10 cm × 10 cm × 500 μm DSSDs and the connection to the readout electronics is through elastomeric connections as opposed to wire-bonds for ease of testing and assembly. The custom packaging designed and built at GSFC is shown here.

The AMEGO tracker prototype that is currently being developed [36] includes 10 layers of 10 cm × 10 cm × 500 μm DSSDs purchased from Micron[2], see **Figure 20**. We have developed custom tracker front-end electronics with the same IDEAS VATA460.3 ASICs (COTS) that will be used for AMEGO. Although the prototype tracker does not include arrays of wire-bonded DSSDs, part of the prototype development will include tests of the DSSDs arranged in an 'L'-shape ladder to understand the noise contributions of this design.

The AMEGO 4 × 4 wire-bonded arrays of DSSDs has been further validated via the MEGA [31] tracker prototype [37] which used almost identical DSSDs, wire-bonded connections, and a composite rib structure as mechanical support. A 2 × 2 wire-bonded array of 2 mm thick DSSDs which also has a similar mechanical support with 8 layers has been previously developed and tested as a Compton telescope in a laboratory setting [38]. Based on this heritage and current technology developments, we have assessed the AMEGO DSSD tracker to be at TRL 6.

Low-Energy Calorimeter: Most of the components of the Low-Energy CZT Calorimeter have high flight heritage from missions such as *Swift*, AstroSat,

[2]http://www.micronsemiconductor.co.uk

NuSTAR, RHESSI, INTEGRAL-SPI, as discussed in **Section III.1.1.11**. The AMEGO detector use a virtual Frisch-grid readout on a 4 cm thick detector, as discussed in **Section III.1.1**. However, this design does not have flight heritage.

A Low-Energy Calorimeter prototype is currently in development. This work is funded through APRA (PI: Thompson) and is being performed by GSFC and Brookhaven National Laboratory (BNL), the two main teams which will design and build the AMEGO CZT calorimeter. The prototype CZT bars are slightly smaller in size, each measuring 0.6 cm × 0.6 cm × 2 cm. The mechanical structure for the circuit-board array, which is the same as proposed for AMEGO, has been designed and tested in the laboratory, see **Figure 21**. The readout for this prototype calorimeter is currently using the AVG2 ASIC [39]. Detector level testing indicates that the requirements for the CZT subsystem are being met [23, 40]. However, it was through initial tests of these detectors that we determined a wave-front sampling ASIC is required to meet AMEGO performance. Therefore, we have base-lined the IDEAS IDE3421 ASIC (COTS) chip for the AMEGO mission, where this family of ASICs has flight heritage (see **Section III.1.1.11**).

Overall the Low-Energy CZT Calorimeter, we have assessed to be at TRL 4, which is driven by the design geometry of the CZT bars.

Prior work indicates that these detectors meet the requirements for AMEGO and the main work needed is raising the TRL. To achieve this, we plan to use a standard path through studies performed on the AMEGO prototype development. We will perform CZT environmental testing to General Environmental Verification Specification (GEVS). In summer 2020, the full AMEGO instrument prototype, including the CZT calorimeter, will be validated in a beam test which will raise the subsystem to TRL 5. The design will be further tested on a balloon flight through the same APRA in fall 2021. We have be rewarded APRA funding (PI: A. Moiseev) to perform environmental testing of the CZT calorimeter subsystem according GEVS. Its success will result in this instrument subsystem achieving TRL 6 prior to Phase A of the AMEGO mission.

High-Energy Calorimeter: The design of the High-Energy CsI Calorimeter relies heavily on the design of the *Fermi*-LAT, which has been operating successfully on-orbit for more than 11 years. The major elements have flight heritage from *Fermi*-LAT, SIRI, Astro-H, eXTP, and CALET, as discussed in **Section III.1.1.11**.

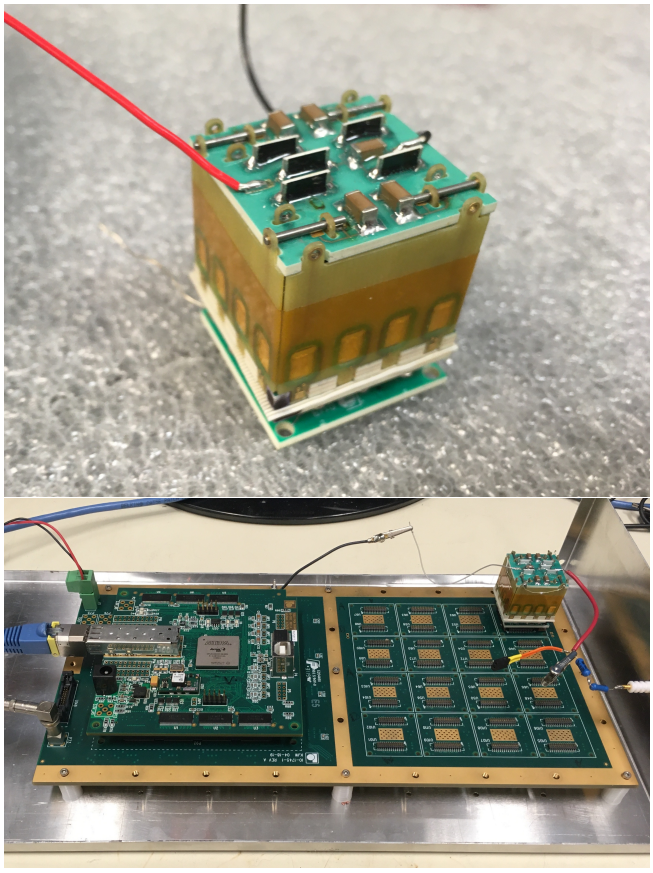

Figure 21: The AMEGO Low-Energy Calorimeter prototype is being developed by Brookhaven National Laboratory and Goddard Space Flight Center. *Top* A single CZT array filled with 4 × 4 CZT virtual Frisch-grid bars. The crate composed of circuit-board material provides the mechanical structure and electrical connection to the electrodes. *Bottom* The CZT arrays, each 16 CZT bars, have been tested on the prototype motherboard using an AVG2 ASIC developed at BNL.

The AMEGO high-energy calorimeter design dramatically improves the low energy performance of the *Fermi*-LAT design by reading out the scintillation light with silicon photomultipliers (SiPMs). The NRL team, who designed and built the *Fermi*-LAT calorimeter, is uniquely qualified to leverage the experience gained from that effort for AMEGO. The High-Energy CsI calorimeter development has been funded through APRA (PI: Grove, PI: Woolf). The prototype consists of thirty 17 mm × 17 mm × 100 mm CsI crystals arranged in

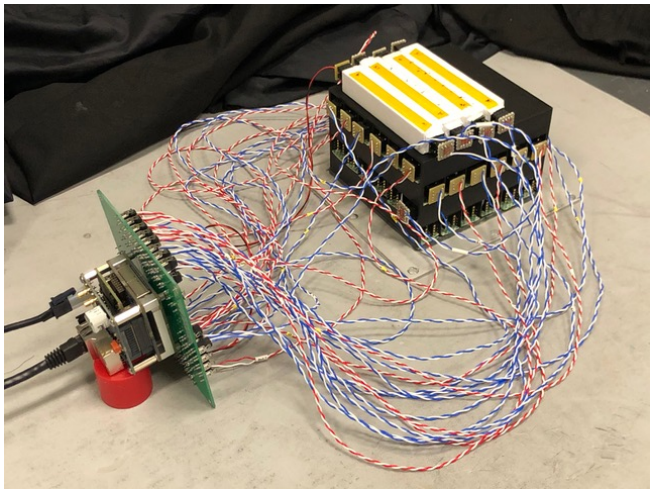

Figure 22: The AMEGO High-Energy Calorimeter prototype is being developed at the Naval Research Laboratory. Shown in the photograph is the partially populated prototype of the CsI calorimeter subsystem. The signal out from each SiPM is connected to the IDEAS ROSSPAD interface board for data handling and event processing.

a five layer (six crystals per layer) hodoscopic structure. Each CsI crystal is wrapped in a diffuse reflector that helps pipe the scintillation photons and each crystal is read out at each end by a 2×2 array of SiPMs, totaling 60 channels for the prototype calorimeter. The SiPMs are read out by the IDEAs SIPHRA ASIC which has similar flight heritage to the currently baselined VA32TA6 III.1.11. The SIPHRA has similar power and performance requirements and can easily be used on AMEGO. The prototype has been built, tested and initially calibrated in the laboratory (see **Figure 22**) and at a first beam test [25]. The performance of the prototype has exceeded the AMEGO requirements. Based on the heritage and current technology developments, we have assessed the High-Energy CsI Calorimeter to be at TRL 6.

Anti-Coincidence Detector: The AMEGO ACD relies heavily on the design of the *Fermi*-LAT, which has been operating successfully on-orbit for more than 11 years. The major elements have flight heritage from *Fermi*-LAT, SIRI, Astro-H, eXTP, and CALET, as discussed in **Section III.1.11**.

The GSFC team conceived, designed, developed, assembled, tested, and currently operates the *Fermi*-LAT ACD and is uniquely qualified to leverage the experience gained from that effort for AMEGO. This work is being advanced through the AMEGO prototype development at GSFC. A five-panel plastic scintillator ACD, with wave-length shifting bars and a SensL-J series SiPM readout, is being built for the prototype balloon flight in fall 2021. Based on the heritage and current technology developments, we have assessed the ACD to be at TRL 6.

III.1.3 Instrument Risks

In the area of instrumentation, what are the top five technical issues or risks?

Risk 1. Instrument Assembly and Test: The assembly and test of this number of DSSD detectors into segments with their associate readout electronics and integrating the segments into towers is a complicated process thus there is a possibility that the assembly could take longer than expected resulting in an overall schedule delay.

Mitigation:

- We have partnered with an assembly facility (Argonne National Laboratory) with known expertise and a proven track record in assembling detectors of this type in these numbers and has capacity in excess of our schedule requirements.
- We have conservatively scheduled a single assembly line and the assembly facility can operate multiple assembly lines if needed (**Figure 30**).
- We have included tolerances for failure of individual detector segments within the science graceful degradation plan.
- We have scheduled for assembly and testing of spare tracker segment layers to compensate for expected yield rate and non-compliant tower segment sub-assemblies.
- We have included sufficiently funded schedule reserve in the tracker assembly to accommodate delays.

Risk 2. Single source DSSD Procurement: We have baselined a single DSSD provider and there is a possibility that they will not produce DSSDs in the mid-2020s resulting in the project having no source of Si DSSDs.

Mitigation:

- We will work with the provider (Hamamatsu) over the next few years to keep them appraised of our status.
- We will procure small batches prior to Phase A to ensure production continuity.

- We will research other manufacturing options prior to Phase A and/or during Phase A.
- We will procure samples from other vendors during Phase A to evaluate their capabilities.

Risk 3. CZT TRL Raising by PDR: The CZT bars are TRL 4 and there is a possibility that the TRL will not be raised to 6 by PDR resulting in a schedule delay and extra cost to the mission.

Mitigation:

- We will test a 16 module prototype prior to phase A in a beam and on a balloon. This effort is fully funded.
- We will build and test a complete structural mass model of an array and an engineering model consisting of four CZT modules in Phase A, and a full tower mass model in Phase B prior to PDR (**Figure 28**).

Risk 4. Load Stress on Tracker DSSD Wafers and Support Structure. A complete analysis of launch acoustic loads (drum effect) and quasi-static loads on the DSSD wafers and composite support structure has not been completed and the loads might exceed structural margins resulting in the need to add more structural supports.

Mitigation:

- We will conduct a complete FEM structural and acoustic analysis of 1 of 4 Tracker towers (all 60 layers) prior to the PDR.
- We will install a cross strap brace over top of the tracker to provide additional rigidity.
- We will design the tracker and build it to provide appropriate atmospheric vent paths.
- We will fabricate a segment mass model with wire-bond traces and do acoustic and vibration testing at protoflight levels in Phase A.

Risk 5. Long lead procurement of DSSDs: Production of DSSDs is complicated and we require a significant number thus there is a possibility that the vendor will not deliver on time resulting in a schedule delay.

Mitigation:

- We will build an engineering model during Phase A to verify the manufacturer's production line (**Figure 28**).
- We will initiate the procurement process and contract negotiations 2 months prior to Phase B (**Section VI.3**).
- We have assumed significant lead time prior to the first DSSD batch delivery (10 months after a 100 day procurement process).
- We have included an adequate (vendor confirmed) delivery window (470 days).
- We can absorb delays in the schedule since the final two towers are to be built after the final delivery and it takes 6 months to assemble a single tower.
- We have included funded schedule reserve at the tower assembly level.
- We will define the procurement strategy 60 days prior to approval to proceed.

III.1.4 Instrument Table

Fill in entries in the Instrument Table. Provide a separate table for each Instrument (Inst 1, Inst 2 etc). As an example, a telescope could have four instruments that comprise a payload: a telescope assembly, a NIR instrument, a spectrometer and a visible instrument each having their own focal plane arrays. Please identify the basis for the CBE (Current Best Estimate).

The AMEGO instrument is summarized in **Table 4**.

III.1.5 Contingency

If you have allocated contingency please describe it, along with the rationale for the number chosen.

Instrument Mass Contingency: The lowest maturity components are the Main Chassis and detector support structure, as well as the Detector Front End Electronics (FEE) and corresponding Pigtail Assemblies, which require TRL 6 raising, or environmental and functional testing at relevant environment. And considering its placement at the current life cycle, a 30% and 25% contingency has been applied, respectively. The highest mass element in the AMEGO instrument is the High-Energy Calorimeter. The dense CsI bars in this subsystem are a simple crystalline material and have known dimensions with small tolerances. As a result, the mass contingency on the non-structural elements should be significantly lower than 25%. Conservatively, an average of 8% contingency has been applied to all other systems based on minimal changes and their heritage-based high TRL.

Instrument Power: Power consumption of all components are well characterized based on high heritage (>TRL 6) flight components and scaling. In

Table 4: AMEGO Instrument table

Item	Value
Type of Instrument	Compton/Pair Telescope
Number of channels	156,400
Size/dimensions (for each instrument)	1.638m×1.638m×1.151m
Instrument mass **without** contingency (CBE*)	1077 kg
Instrument mass contingency	10 %
Instrument mass **with** contingency (CBE+reserve)	1183 kg
Instrument average payload power without contingency	1119 W
Instrument average payload power contingency	15 %
Instrument average payload power with contingency	1287 W
Instrument average science data rate without contingency	4192 kbps
Instrument average science data rate contingency	20 %
Instrument average science data rate with contingency	5030 kbps
Instrument Fields of View (if appropriate)	130°
Pointing requirements (knowledge)	0.0083°
Pointing requirements (control)	5°
Pointing requirements (stability)	N/A

addition, a detailed concept of operations profile has been created from which average and peak power estimates have been derived. But considering the instrument is at Pre-Phase A, a conservative 15% contingency has been applied to the average power, with ample margin when handling peak consumption, such as during a solar flare event.

Instrument Data Rates: Instrument data rates are derived from the average number of detection events per second (3K/sec from simulations), and peak rates based on an operational event, such as a solar flare where additional ACD detections would take place. Based on variability of number of detection and its placement in its life cycle, a 20% contingency has been applied.

III.1.6 Organizational Responsibilities

If known, provide a description of what organization is responsible for each instrument and summarize relevant past experience with similar instruments.

Tracker: Argonne National Laboratory (ANL) and Goddard Space Flight Center (GSFC). ANL will be responsible for the Assembly, Integration and Test of the Silicon tracker towers, leveraging their extensive facilities, expertise and experience with large-scale silicon detectors for Large Hadron Collider experiments. GSFC will be responsible for the mechanical structure, leveraging extensive flight expertise in composite materials. Additionally, GSFC has extensive flight experience building and testing silicon trackers for instruments both on-orbit and in balloon payloads. GSFC has led the design, development and testing of the AMEGO tracker prototype. The team also includes experts in silicon tracker instrumentation at the Naval Research Laboratory and University of California, Santa Cruz.

High-Energy Calorimeter: Naval Research Laboratory (NRL). NRL led all aspects of the CsI calorimeter on Fermi – from development through calibration and operation. The CsI calorimeter on AMEGO is very similar. The High Energy Space Environment (HESE) Branch at the Naval Research Laboratory (NRL) has been conducting leading-edge research in gamma-ray astrophysics and gamma-ray detector systems since the early 1970s. Members of the Branch participating in AMEGO instrument design and development were members of the PI team for the Oriented Scintillation Spectrometer Experiment (OSSE) on the Compton Gamma Ray Observatory, and they conceived, designed, and built the Calorimeter subsystem for the Fermi Large Area Telescope (LAT). Laboratory, clean room, and environmental testing facilities for the *Fermi*Calorimeter and LAT construction and testing are available for use in AMEGO. HESE Branch members contributing to AMEGO have extensive experience across a broad range of semiconductor and scintillation detector systems for terrestrial and space application,

and have successfully delivered and operated multiple space-based gamma-ray instruments for DoD, NASA, and other government sponsors.

Low-Energy Calorimeter: Brookhaven National Laboratory (BNL) and GSFC. BNL has over seven decades of experience in developing large scale particle detectors in their instrumentation division. Specifically, this division is the originator of the virtual Frisch-grid CZT detectors baselined for AMEGO and has developed the front end electronics for the prototype CZT bar detectors. GSFC has extensive flight experience building large-scale CZT detector arrays for instruments on-orbit (*Swift*-BAT). GSFC has also led the mechanical structure, testing and integration of the AMEGO CZT calorimeter prototype.

Anti Coincidence Detector: Goddard Space Flight Center. The GSFC team successfully designed and built the *Fermi*-LAT ACD. GSFC has also led the design of the AMEGO ACD prototype.

DAQ/FSW: Los Alamos National Laboratory With nearly six decades experience from more than one hundred National Security Space Missions and NASA Missions, Los Alamos National Laboratory (LANL) has extensive experience within the development, deployment and operation of flight software. And to support those efforts, LANL has a team of about 50 software engineers and scientists with solid flight software experience. Recent example of LANL's successful development of flight software for NASA gamma-ray astronomy missions are the real-time, on-board, gamma-ray burst localization software packages LANL created for the *Swift* and HETE missions.

Detector Simulations and Pipeline Algorithm Development: University of California Berkeley. Dr. Andreas Zoglauer from UC Berkeley's Space Sciences Laboratory leads the development of MEGAlib, the Medium-Energy Gamma-ray library, which is the foundation of the simulation and data analysis pipeline of the COSI balloon telescope [41]. MEGAlib was originally developed for the MEGA combined Compton and pair telescope [42], and is therefore well-suited as the base for developing the AMEGO simulation and data analysis pipeline.

The work breakdown described above assumes an entirely US funded mission. However, AMEGO is a large international team and our expectation is that there will be significant contributions and hardware responsibilities provided by our non-US team members. In particular, subject to passing appropriate review and approval, we plan to leverage extensive Italian expertise in Assembly, Integration and Test of silicon trackers with an expectation that our Italian partners will play a major leadership role in the silicon tracker subsystem. We plan to explore French contributions to the tracker front-end electronics using the IDeF-X ASIC developed at CEA/Saclay. This ASIC has been selected for the STIX instrument of the Solar Orbiter mission.

III.1.7 Studies Performed

For the science instrumentation, describe any concept, feasibility, or definition studies already performed.

The team participated in an instrument and mission design lab at GSFC for a similar mission concept to AMEGO (called ComPair). For the ComPair mission and to develop the proposal for the MIDEX AO, the instrument went through full development, design and costing at GSFC. ComPair included slightly smaller versions of three of the four major subsystems: the tracker, the High-Energy (CsI) Calorimeter and the ACD. The ComPair concept was not proposed because the modeled cost of the spacecraft pushed the overall mission cost too high to be accommodated as a MIDEX.

As part of the preparation for this RfI, we also received additional engineering support at GSFC to scale up the instrument subsystems from the ComPair design to accurately estimate mass and power. Additionally, we developed a robust mechanical and electrical design for the Low-Energy CZT Calorimeter.

III.1.8 Calibration and Data Plan

For instrument operations, provide a functional description of operational modes, and ground and on-orbit calibration schemes. Describe the level of complexity associated with analyzing the data to achieve the scientific objectives of the investigation. Describe the types of data (e.g. bits, images) and provide an estimate of the total data volume returned.

The AMEGO science goals are achieved primarily through survey-mode observations, where the wide field-of-view allows for the full sky to be observed

every 3 hours. **Section III.2.1** describes the operational modes in detail.

The ground calibration plan and in-orbit calibrations will be based off of *Fermi*-LAT and lessons learned from the AMEGO prototype development, CGRO/COMPTEL [43], and COSI instrument [44]. In addition to understanding the conversion of pulse height and timing of interactions into energy and position within the instrument, calibration measurements are vitally important for benchmarking the simulation tools.

Many of the full-instrument calibrations can be done in-orbit during normal survey-mode observations. Measurements taken in orbit can be used to refine the simulated response of the instrument better than what is achievable through ground calibrations. The alignment calibration of the tracker and calorimeters can be done with cosmic-ray charged particles, which will leave straight tracks through the instrument. These minimum ionizing particles (MIPs) deposit a known energy and will be used to monitoring the gain of the High-Energy Calorimeter. The gain of the Low-Energy Calorimeter can be monitored with the 511 keV background line and other internal activation lines, while the tracker can be calibrated with the charge injection capability from the DSSD ASICs. The absolute pointing of AMEGO can be determined through observations of bright gamma-ray point sources, such as the Crab Nebula, Vela pulsar and bright AGN from the *Fermi* catalog [45]. Absolute timing calibrations can be done with bright pulsars, such as the Vela pulsar and Crab pulsar. A calibration on the imaging performance can be performed with bright gamma-ray sources to verify effective area and angular resolution throughout the field-of-view. There are no additional pointed observations that are needed for these calibrations, as science data that is taken during survey-mode observations provide adequate statistics for whole sky.

The main calibration of each subsystem is performed at the module level prior to integration using sealed radioactive laboratory sources that span the energy range from 30 keV to 1.8 MeV (e.g. ^{241}Am, ^{133}Ba, ^{137}Cs, ^{57}Co, ^{60}Co, ^{22}Na, and ^{88}Y). These measurements will allow for a calibration of the energy and position response of the DSSD tracker, the Low-Energy CZT Calorimeter, and the High-Energy CsI Calorimeter. More refined calibrations of the cross-talk and charge sharing between neighboring strips in the DSSDs and a precise calibration of the Low-Energy CZT Calorimeter can be done with these on-the-bench measurements.

Post CDR, the ETU tower will be available for benchmarking and validating the Monte Carlo simulations prior to instrument integration. This will include a test at a high energy electron beam to test the high-energy response of the calorimeter, and a polarized gamma-ray beam to test the polarization response of all subsystems together. Once the flight instrument is integrated, we will continue to monitor the energy response of all subsystems with sealed radioactive laboratory sources. Cosmic-ray muons allow for alignment and gain monitoring of the High-Energy Calorimeter.

The data for AMEGO is event-based, where each gamma-ray interaction in the instrument is analyzed separately. Images, light curves, polarization analysis, and other science products are generated on-ground. The raw data for each event, including housekeeping and aspect information, is telemetered down as the Level 0 data (described further below) and the expected data rate is 5.0 Mbps.

AMEGO has 6 levels of science data products. The Level 0 data product is telemetered down from the spacecraft. This includes the raw data (ADC and timing of signals from each trigger), aspect information, and house keeping. On the ground, it will be unpacked and automatically converted into the FITS format which then represents Level 1 data. The first analysis step is the measurement calibration, which includes energy, position, and depth calibration, etc. The resulting Level 2 data is a list of events consisting of calibrated detector hits (energy, position), (interpolated) instrument aspect information, absolute time, etc. The next step in the analysis encompasses the identification of the event type (Compton, pair, charged particle, etc), the tracking of electrons and positions in the tracker and eventually down to the calorimeter, the determination of the overall Compton sequence and an overall quality factor of the event (see e.g. [30] for an overview). This stage results in Level 3 data consisting of the reconstructed primary event parameters as a photon list such as the direction of the pair electron and positron, the sorted Compton interaction sequence, and so on. This data set (along with appropriate response files) is the start point for all high-level

data analysis which most science user will use for their analysis: all-sky imaging, source identification, spectral fitting, polarization analysis, etc. Level 4 data will be the result of an automated analysis of the measured data and include all-sky images, lists of bright sources containing locations, spectra, light curves, for different time intervals, etc. Level 5 data will consist of catalogs of reviewed Level 4 data. The AMEGO team will produce a catalog of gamma-ray sources, flux histories and tentative source identifications, as well as all-sky maps for continuum observations and gamma-ray line emissions.

Figure 23 shows an overview of the data flow and the data products. In general, the same pipeline will be used to analyze the on-orbit observations, ground calibrations, and simulations. Well-benchmarked simulations are a key element to generate accurate response files and, e.g., trained neural networks to identify the event type and the hit sequence. To achieve a good agreement, the detector effects engine, which handles mass model, energy and position resolution, triggers, etc. is tuned to produce simulated events which are as similar as possible to the observations. At each step of the analysis pipeline measurements and simulations of the same observation/calibration can be compared. Differences between the two will inform updates/improvements to the detector effects engine. The presented pipeline is largely identical to the already existing simulation and data analysis pipeline which is used for COSI [46] as well as for the AMEGO performance simulations (see **Sections III.1.1**). Both utilize the open-source MEGAlib toolkit [27], which will also be the base of the final AMEGO simulations and data analysis pipeline.

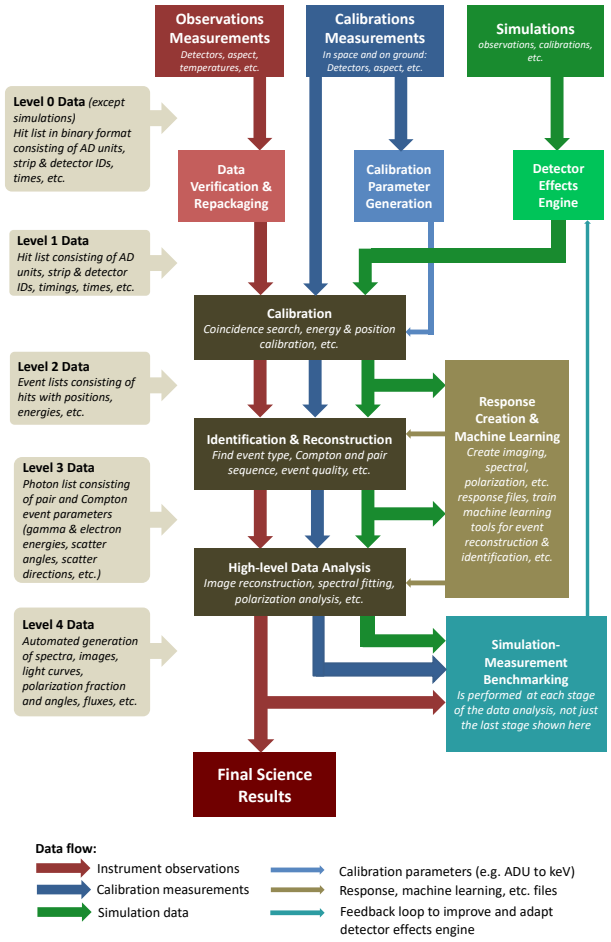

Figure 23: The proposed AMEGO pipeline is largely identical to the already existing data pipeline used for COSI and the AMEGO performance simulations. Shown here is an overview of data flow and products for AMEGO observation, calibrations, and simulations which is based on the MEGAlib toolkit.

III.1.9 Instrument Flight Software

Describe the level of complexity of the instrument flight software.

The AMEGO flight software is straightforward as no on-board event reconstruction is required. For general science observations, Level 0 raw data is transmitted to ground as described **Sec. III.1.8**. For transient detections, AMEGO flight software includes algorithms for onboard GRB triggering. The option of including a simplistic on-board reconstruction in the pair-regime, such as what is done in *Fermi*-LAT, to reduce the background data rate will be explored in Phase A.

For development of the AMEGO flight software, LANL will employ a similar strategy to the one LANL very successfully used for NASA's *Swift* Mission. The software will be developed in C++ using POSIX standard interfaces and restricted as appropriate for a high-reliability embedded system (e.g. no exceptions; no heap memory allocation except for a fixed set of buffers at boot time). Confidence that the software will Do The Right Thing will be provided by extensive simulation and testing under non-deterministic conditions. The development/test hardware will be a single-board computer, with ground station and WFI front-end electronics simulators running under virtualization on a single desktop computer. This will allow testing

of commanding, data telemetry, and automation as well as simulation of the detector hardware, slewing mount, and the external universe. For the highest fidelity testing, we will employ an Engineering Test Unit, a flight-like hardware unit, along with the associated ground station and simulation computers. This, combined with the extensive use of heritage code and experience, will allow LANL to confidently deliver reliable flight software.

III.1.10 Non-US Participation

Describe any instrumentation or science implementation that requires non-US participation for mission success.

No non-US participation is required for mission success and the baseline instrument described here assumes no non-US participation. However, contributions from our European and Japanese partners will make the mission significantly stronger and are expected.

III.1.11 Instrument Flight Heritage

Describe the flight heritage of the instruments and their subsystems. Indicate items that are to be developed, as well as any existing hardware or design/flight heritage. Discuss the steps needed for space qualification. Describe any required deployments.

The AMEGO design is based on having flight heritage and experience for every instrument subsystem and relies heavily on the *Fermi*-LAT design; however, there are some key differences since AMEGO is optimized for lower energies. For example, the AMEGO tracker has been modified to detect low energy pair conversion events and the Compton-scattered electron by both removing the high-Z Tungsten converter foils and changing from single-sided to double-sided silicon strip detectors. The former reduces multiple scattering which improves the angular resolution of the instrument, while the latter allows two dimensional position resolution within the same bulk material. AMEGO has the addition of a Low-Energy CZT Calorimeter optimized for the Compton regime with high spectral resolution. The energy resolution of the CsI calorimeter is improved with respect to the LAT by using solid state SiPMs instead of PIN diodes; however, because of the low energy focus it is fewer radiation lengths deep. Finally, due to the lower energy of AMEGO, the ACD is not segmented into multiple tiles per side. Further details on the heritage for each subsystem are given below.

Tracker: All major components of the AMEGO tracker have flight heritage from missions including *Fermi*-LAT, AMS-02, Astro-H, PAMELA, and others.

Each tracker segment is identical and contains a 4×4 array of wire-bonded DSSDs. DSSDs have flight heritage on AMS-02 [47, 48], Astro-H HXI [49], and PAMELA [50, 51]. Daisy-chained DSSDs connected via wire bonding have been demonstrated on AMS-02 and PAMELA, although the dimensions of the wafers are different.

The mechanical design of the tracker uses Carbon Fiber Reinforced Polymers (CFRP) which have been successfully implemented on *Fermi*-LAT, HST, JWST, Ice-Sat and many other space missions. The DSSDs are suspended in a grid of CFRP ribs that also hold an 'L' shaped front-end electronics board. A mechanical rib support structure of composite materials that is similar to the AMEGO design has been flown on PAMELA. Mechanical fasteners are included at nodes in the segment to allow for stacking, which has also been demonstrated on both and AMS-02 and PAMELA.

Due to the large number of components and the complexities in integration, significant effort was made in the design to make each component identical and interchangeable. A very similar tracker tower construction of daisy chained silicon detectors, although single sided wafers, was flown on *Fermi*-LAT.

For the analog read-out electronics, we have bench-marked the IDEAS VATA460.3 (COTS). This family of ASICs has flight heritage on Astro-H [52] and IDEAS has produced flight hardware for over a decade.

Low-Energy Calorimeter: The components of the Low-Energy CZT Calorimeter have high flight heritage from missions such as *Swift*, AstroSat, *NuSTAR*, RHESSI, INTEGRAL-SPI, and many others.

CZT pixel detectors have flown on *Swift*–BAT [53], *NuSTAR* [54], and AstroSat [55]. The main difference between these instruments and the AMEGO design is the detector geometry. The AMEGO detector use a virtual Frisch-grid readout on a 4 cm thick detector, as discussed in **Section III.1.1**. However, this design does not have flight heritage.

The CZT bars are loaded into a module of 4×4 bars, and the structure is made of PCB with electrical traces providing the contact to the CZT side terminals via spring loaded contacts. Electrical contacts between the CZT bar electrodes and the readout electronics are via spring loaded contacts, which have high heritage (i.e. slip rings). We are unaware of printed circuit boards as mechanical structure; however, PCBs are ubiquitous and undergo extensive mechanical analysis for every mission, so use in this manner is low risk. The design allows for alternative material (such as Kapton), if necessary.

The readout electronics for the Low-Energy Calorimeter utilizes the IDEAS IDE3421 ASIC (COTS). The COTS ASIC is based on a family of ASICs with flight heritage and is designed by a company that specializes in ASICs for flight applications. The modular socket connection of each CZT module to the motherboard has been demonstrated on the *Swift*-BAT. Additionally, the 4 kV bias voltage required for these 4 cm thick CZT bars has been demonstrated on RHESSI [56] and INTEGRAL-SPI [57].

High-Energy Calorimeter: The design of the High-Energy CsI Calorimeter relies heavily on the design of the *Fermi*-LAT, which has been operating successfully on-orbit for more than 11 years. The major elements have flight heritage from *Fermi*-LAT, SIRI, Astro-H, eXTP, and CALET.

The CsI(Tl) crystal scintillators in a hodoscopic array have been demonstrated with the *Fermi*-LAT calorimeter. The use of composite materials for the mechanical design will be the same as for *Fermi*-LAT. In AMEGO, silicon photo-multipliers (SiPMs), which replace the PIN diodes used in the *Fermi*-LAT design. The SensL-J series SiPMs used for AMEGO have demonstrated on-orbit performance with SIRI [58] and will be also flown on BurstCube [59].

The High-Energy Calorimeter read-out electronics have been designed using the IDEAS VA32TA6 ASIC [3]. These ASICs have flight heritage on Astro-H, eXTP [60], and CALET [61].

Anti-Coincidence Detector: The AMEGO ACD relies heavily on the design of the *Fermi*-LAT, which has been operating successfully on-orbit for more than 11 years. The major elements have flight heritage from *Fermi*-LAT, SIRI, Astro-H, eXTP, and CALET.

The AMEGO ACD is a simplified version of the *Fermi*-LAT ACD: there is no segmentation of the panels (as it is not required at low energies) and there are no wavelength-shifting fibers embedded in the detector material. The detector material (plastic scintillator) has extensive flight heritage including *Fermi*-LAT and many other instruments previously flown and currently flying. As with the CsI calorimeter, the ACD plastic scintillators use a SensL-J series SiPM readout, which have been demonstrated on orbit with SIRI [58] and will be further tested BurstCube [59]. The read-out electronics use the IDEAS VATA64HDR16 ASIC (COTS) which are part of a family of ASICs that have flight heritage on Astro-H, eXTP [60], and CALET [61].

III.2 Mission Design

Please answer the following, or point to pages in existing public documentation where the information is provided:

III.2.1 Science Driven Mission Requirements

Provide a brief descriptive overview of the mission design (launch, launch vehicle, orbit, pointing strategy) and how it achieves the science requirements (e.g. if you need to cover the entire sky, how is it achieved?).

The AMEGO mission design assumes a launch from KSC on a Large Payload Fairing (such as Falcon 9 or Atlas, see **Figure 24**) and directly injected into a 600 km 6° inclined circular orbit. An orbit inclination between 0 and 10° would provide acceptable AMEGO instrument science viewing. However, 6° was selected to minimise the radiation environment encountered during transit through the South Atlantic Anomaly (SAA). AMEGO is unaffected by launch date window restrictions as the science data can be obtained regardless of the orbit RAAN, time of day, or launch date.

AMEGO has two main modes of operation to collect science data. The primary method is a survey operations mode where the observatory's Z-axis is pointed 30° North along the local zenith for one orbit, the observatory is slewed at 0.25 degrees/sec for approximately 240 seconds so that the observatory's

[3] https://ideas.no/launch-of-hxmt-with-ideas-integrated-circuits/

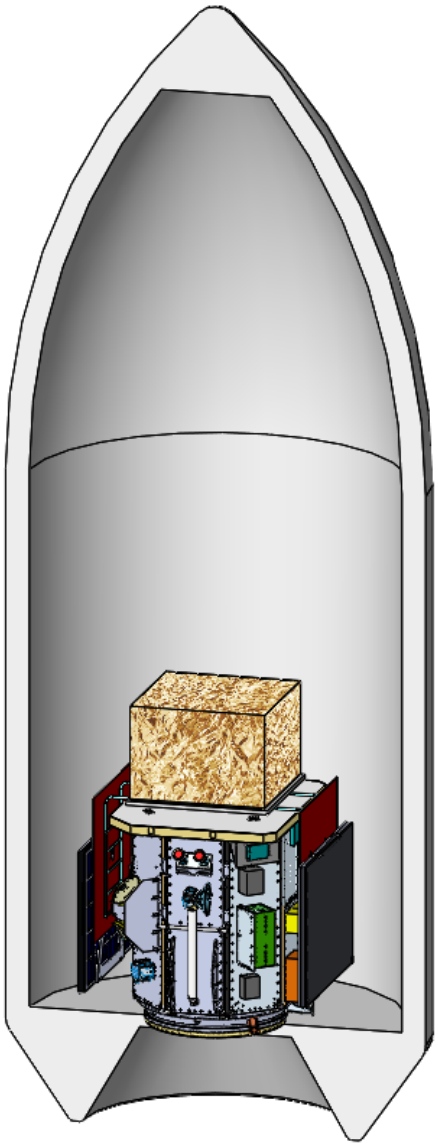

Figure 24: AMEGO fits comfortably in a Falcon 9 fairing with significant clearance. The Falcon 9 rocket can place AMEGO in the desired orbit with sufficient margin (**Table 5**). Shown in the fairing is the single AMEGO instrument externally mounted on a standard LEOStar-3 spacecraft. The two articulated solar panels are in their stowed postion on the right and left of the bus. A gimbled high-gain Ka-band is shown on the facing side of the spacecraft as well as the star trackers (red circles) and other spacecraft components.

Z-axis is pointed 30° South along the local zenith. This process is repeated every orbit to maximize uniformity of sky coverage on timescales of 3 hours (two orbits). The second mode is an inertial target mode, where the observatory follows a target until it gets within 30° of the Earth limb. The Z-axis is then held constant relative to the Earth, so that the target moves through the instrument FoV until occultation (but most of the FoV is still kept off the limb). When the target becomes occulted, the boresight is moved 30° away from the other side of the Earth, where the target is reacquired as it emerges from occultation.

Spacecraft operations does not interfere with science operations in either science mode. In both observing modes, the Observatory is allowed to rotate about the Z-axis to maintain full solar illumination of the solar arrays, and to keep the Sun off the radiators.

The science data volume produced by AMEGO is approximately 45 GB over a 24 hour period. This volume exceeds the capabilities of a typical spacecraft S-band communications subsystem. For this reason, a high bandwidth Ka-band communications subsystem is used to downlink science data while a lower-bandwidth S-band communications subsystem is used for spacecraft and instrument command and telemetry. Due to the lack of Ka-Band ground stations in view of AMEGO's low inclination orbit, NASA's Space Network, specifically TDRS-East and TDRS-West is utilized for nominal operations for both S-band and Ka-band. TDRS-F-7 at 85° in the zone of exclusion is used for S-Band contingency and critical event communications. S-Band communications use a set of omni-directional antennas that provide nearly 4pi-steradian of coverage to TDRSS or a ground network station in view.

Reaction wheels manage observatory momentum. Excess momentum is offloaded with magnetic torquers, eliminating the need for a propellant based reaction control system and any interruptions to science data collection.

The spacecraft includes a propulsion system to allow safe deorbit at the end of the mission.

III.2.2 Mission Software, Ground Station, and Science Development

Describe all mission software development, ground station development and any science development required during Phases B and C/D.

AMEGO does not have any unusually complex or driving mission software. Spacecraft and instrument flight software is straightforward and similar to (or simpler than) what was developed for the Fermi Gamma-ray Space Telescope. The ground system

Table 5: Mission Design Table

Parameter	Value
Orbit Parameters	600 km circular, 6 deg inclination
Mission Lifetime	60 months
Maximum Eclipse Period	36.5 min
Launch Site	CCAFS
Spacecraft Dry Bus Mass without contingency	1,903 kg
Spacecraft Dry Bus Mass contingency	15.1%
Spacecraft Dry Bus Mass with contingency	2,193 kg
Spacecraft Propellant Mass without contingency	352
Spacecraft Propellant contingency	30%
Spacecraft Propellant Mass with contingency	458 kg
Launch Vehicle	Falcon 9 with Full Thrust, Return to Launch Site (RTLS) capability
Launch Vehicle Mass Margin	4,661 kg
Launch Vehicle Mass Margin	121%
Spacecraft Bus Power without contingency	988 W OAP
Spacecraft Bus Power contingency	12 %
Spacecraft Bus Power with contingency	1,105 W

software takes advantage of extensive reuse of existing code.

No ground station development is necessary for AMEGO, as science data downlinks and observatory commanding is via TDRSS Ka-band and S-band contacts.

No science development is necessary beyond the data archiving capability and data analysis software developed by the SOC. This will be similar in scope to what was done for Fermi.

III.2.3 Mission Design Table

Provide entries in the Mission Design Table. For mass and power, provide contingency if it has been allocated. If not, use 30% contingency. To calculate margin, take the difference between the maximum possible value (e.g. launch vehicle capability) and the maximum expected value (CBE plus contingency). **Table 5** provides mission, orbit, spacecraft, and vehicle properties.

III.2.4 Observatory Block Diagrams

Provide any existing block diagrams or drawings showing the observatory (payload and spacecraft) with the instruments and other components labeled and a descriptive caption. Provide a diagram of the observatory in the launch vehicle fairing indicating clearance if you have it.

See **Figure 24** for a diagram of AMEGO integrated with a standard LEOStar-3 spacecraft in the Falcon 9 fairing showing sufficient clearance.

III.2.5 Mission Risks

For the mission, what are the three primary risks?

The AMEGO spacecraft, ground system, mission and science operations are based on significant heritage from *Fermi*. As a result, the mission risks are focused on the instrument. The top three risks are: 1) Instrumemt assembly integration and test, 2) Single source DSSD procurement and 3) CZT TRL Raising by PDR. See **Section III.1.3** for a discussion of these risks and planned mitigation.

III.2.6 Propellant

Provide an estimate of required propellant, if applicable.

The spacecraft has a propulsion system to allow a controlled deorbit at end of life. The estimated propellant mass is 352 Kg without margin (**Table 5**).

III.3 Spacecraft Implementation

Please answer the following, or point to pages in existing public documentation where the information is provided:

III.3.1 Spacecraft Requirements

Describe the spacecraft characteristics and requirements. Include a preliminary description of the spacecraft design and a summary of the estimated performance of the key spacecraft subsystems. Please fill out the Spacecraft Mass Table and Spacecraft Characteristics Table.

The Observatory mass and power table is provided in **Table 6**, and the Spacecraft Characteristics table is **Table 7**.

The AMEGO spacecraft fits comfortably within several vendors' spacecraft platforms available on GSFC's Rapid Spacecraft Development Office (RSDO), Examples are Ball Commercial Platform (BCP) 2000, Loral/SSL 1300 and Northrup Grumman's LEOStar-3. While a spacecraft partner has not been selected for AMEGO, for the purposes of evaluating capabilities and as a proof of concept, we have baselined a LEOStar-3. The LEOStar-3 product line has extensive heritage, most notably including *Fermi*. In comparison to AMEGO, *Fermi* is of the same mission class, has a very similar operations concept, and requires similar payload resources. Since *Fermi's* launch several LEOStar-3 spacecraft of similar complexity have been launched (*ICESat-2* and *Landsat 8*) and are currently in production (Landsat 9 and JPSS-2). The AMEGO spacecraft is a fully redundant RSDO catalog LEOStar-3, which makes extensive use of existing mechanical, thermal, electrical and digital designs from the *Fermi* spacecraft.

Structure and Physical Packaging. The all-aluminum spacecraft bus primary structure is anticipated to be highly similar to the *Fermi* spacecraft configuration. The primary structure consists of upper and lower ring sections separated by vertical longeron tubes. Shear panels close out the structure and support spacecraft electrical components. The mechanical structure also includes a deployable high-gain antenna and two deployable solar array wings (**Figure 24**). The support structure for the propulsion subsystem is a separate modular aluminum structure that can be installed at any time in the spacecraft integration flow. The bottom of the propulsion support structure acts as a launch vehicle adapter and interfaces with a (commonly used) 1,666mm (66-in.) Marmon band interface to the launch vehicle (other adapter interfaces can be utilized).

Electrical Power Subsystem (EPS). The EPS uses a direct energy transfer system that is battery clamped to 25-34 V. It consists of two, 4-panel deployable wing Solar Arrays using 28.5% Emcore BTJ cells. Each solar array wing is driven by a single axis Solar Array Drive Assembly (SADA) which is stepped at a constant rate of roughly 8 Hz with a tapered start/stop rate that prevents excitation of the Solar Array fundamental mode. If necessary, the Solar Array can be further isolated from the SADA and spacecraft by a damper that isolates Solar Array flexible modes from the spacecraft, ensuring non-interaction with the attitude control loop for wide stability margins. A Power Distribution Unit (PDU) distributes power to the spacecraft bus and instrument payload components and controls Solar Array power input to 134 A-hr Li-Ion battery. A Cell Balance Electronics unit maintains voltage balance between the individual Li-Ion battery cell modules, which is required for long-life missions using Li-Ion battery cells. The spacecraft harness distributes power and signal to the spacecraft bus and instrument payload components.

Command and Data Handling (C&DH) Subsystem. The C&DH is comprised of an Integrated Electronics Module (IEM), Payload Interface Electronics (PIE) and a Solid State Recorder (SSR). The IEM utilizes a 6U cPCI-based architecture with a high performance RAD750 processor and with a dual redundant MIL-STD-1553 data bus for instrument data and command transmission, SSR control, and bi-level and digital channels for commands and telemetry. The SSR stores all instrument data. The PIE interfaces the instrument with the SSR and the Ka-Band Transmitter to downlink data to the ground. The oven-controlled crystal oscillator (OCXO) maintains a stable, accurate time base and guarantees clock drift performance in the event of GPS 1 PPS outages.

Attitude Determination and Control Subsystem (ADCS). The LEOStar-3 spacecraft uses a 3-axis stabilized zero-momentum biased attitude control system. The ADCS hardware consists of

six reaction wheels spinning at low speed to provide primary attitude control during all operational modes. Three electromagnetic torque rods with linear drivers are used for momentum unloading, three axis magnetometers provide measurements of the local magnetic field vector for momentum unloading and coarse attitude determination. Three star trackers provide high accuracy attitude knowledge measurements. A Scalable Inertial Reference Unit (SIRU) provides highly accurate three-axis rate information. Twelve Coarse Sun Sensors (CSS) ensure unique sun vector measurements with at least three overlapping FOVs in every direction. GPS receivers are used to obtain ephemeris knowledge and precision timing.

Spacecraft Flight Software (FSW) provides on-board computation and supports ground command and Observatory telemetry implementation. It manages the redundant interface to all the devices connected through the C&DH subsystem and is the primary interface to the ADCS. The FSW executes on a BAE Systems RAD750 Central Processing Unit (CPU). The FSW consists of four components. The first is the VxWorks Real-Time Operating System (RTOS) that provides top-level task scheduling, prioritization, and preemption capability. The ADCS FSW is developed using MathWorks Simulink^{TM} visual control diagrams and automatically generated by using the MathWorks Real-Time Workshop^{TM} (RTW) Embedded Coder. The stellar navigation FSW, provided by the Star Tracker supplier is also hosted on the RAD 750. Finally, the C&DH FSW (fourth component) is hand coded in C/C++ and compiled using a GNU compiler. It contains the remaining FSW functionality and provides the interface to other spacecraft components as required.

Telecommunications (Telecomm) Subsystem. The Telecomm subsystem features an S-Band narrowband system for telemetry and command services, and a Ka-Band wideband system for high rate downlink of science data. The narrowband system uses a pair of S-Band transceivers with the transmitter feeding its own pair of summed nadir/zenith antennas. The same is true for the receive side. The command receiver demodulates the signal from the TDRSS followed by a Non-Return to Zero conversion from Mark to Level. Recovered data is aligned with an embedded synchronization mark which allows the Crypto block boundaries to be isolated for AES decryption and authentication. If the message is authenticated, it is output to the C&DH subsystem. If not, the message is discarded. There is no bypass or clear channel. The Ka-Band wideband subsystem transmitter takes the science data stream outputs from the PIE. The transmitter RF outputs to a 150W Traveling Wave Tube Amplifier (TWTA), operating at 65 watts RF power, with a hybrid coupler to a DSN Filter. The output can be configured to either a pair of Earth Coverage Antennas or to a two axis steerable narrow beam antenna.

Propulsion Subsystem The propulsion subsystem provides ΔV for propulsive maneuvers for collision avoidance and controlled de-orbit. The subsystem consists of a propellant tank, with a diaphragm for propellant management and slosh control, service valves, filter(s), redundant latch valves, redundant pressure transducers and flow orifices. The system is configured with eight 22N thrusters and four 5N thrusters. It is a fully welded and radiographically inspected system. The 22N thrusters are sized for a final de-orbit maneuver assuming one failed thruster, with thrust levels large enough to avoid large gravity losses during the final burn. The four 5N thrusters are used to perform collision avoidance maneuvers.

Thermal Control Subsystem (TCS) The TCS is a semi-passive design that satisfies all instrument thermal requirements and maintains all spacecraft components within flight-allowable temperature limits. It utilizes constant conductance heat pipes, Multi-Layer Insulation (MLI) blankets, heaters (both software and thermostatically controlled), thermal isolators, and low absorptivity/high emissivity radiators. The instrument optical bench is configured to minimize the spacecraft thermal back loading on the instrument. Low conductivity spacers, struts, and flexures are used to thermally isolate the instrument optical bench from the spacecraft.

Table 6: Observatory Mass and Power Summary

Subsystem	**CBE (kg)**	**Percent Mass Contingency (%)**	**CBE Plus Contingency (kg)**	**CBE Power (w OAP)**	**Power Contingency (%)**	**CBE Plus Contingency (w OAP)**
Structure & Mechanisms	951	20%	1,142	0	0%	0
Power (incl. Harness)	576	10%	634	250	5%	262
Propulsion	63	5%	67	1	3%	1
Attitude Control	109	10%	120	129	20%	155
Command & Data Handling	50	3%	52	140	10%	154
Communications	36	3%	37	280	10%	308
Thermal	118	20%	141	188	20%	225
Total Spacecraft (Dry)	1,903	15%	2,193	988	12%	1,105
Instrument Accommodation	1,077	10%	1,183	1119	15%	1,287
Observatory (Dry)	2,980	13%	3,376	2,107	14%	2,392
Maximum Propellant	352	30%	458	–	–	–
Pressurant	4	20%	5	–	–	–
Total Observatory (Wet)	3,336	15%	3,839	2,107	14%	2,392
Falcon 9 (Full Thrust, RTLS) Performance to 600 km × 6 degree inclination			8,500			
Launch Mass Margin			4,661 kg			
Launch Mass Margin			121%			

Table 7: Spacecraft Characteristics Table

Spacecraft Component	**Value/Summary, Units**
Structure	
Structures material (aluminum, exotic, composite, etc.)	Spacecraft primary structure consists of extruded and sheet aluminum and aluminum honeycomb, Solar panels are constructed with carbon fiber face sheets with aluminum honeycomb
Number of articulated structures	3 – two solar array wings each driven by a single axis gimbal and one Ka-Band narrow beam antenna mounted to a two-axis gimbal
Number of deployed structures	3 – two solar array wings and one Ka-band narrow beam antenna
Thermal Control	
Type of thermal control used	Cold-biased semi-passive design utilizing constant conductance heat pipes, Multi-Layer Insulation (MLI) blankets, heaters (both software and thermostatically controlled), thermal isolators, and low absorptivity/high emissivity radiators. As implemented on the *Fermi* spacecraft, the spacecraft to instrument interface is thermally isolated. Heat transfer across the interface is typically on the order of 5W.
Propulsion	
Estimated delta-V budget, m/s	ΔV = 232 m/sec (based on the Rocket Equation) Isp = 200 sec Initial maximum wet mass mo = 3,839 kg Maximum propellant mass mp = 458 kg

Continued on next page

Table 7: Spacecraft Characteristics Table

Spacecraft Component	**Value/Summary, Units**
Propulsion type(s) and associated propellant(s)/oxidizer(s)	monopropellant blow-down hydrazine
Number of thrusters and tanks	One diaphragm-type propellant tank, eight 22N (5 lbf) thrusters (MR-106L) and four 5N (1 lbf) thrusters (MR-111G). Propellant tank maximum propellant load is 458 kg
Specific impulse of each propulsion mode, seconds	Nominal Isp for the MR-106L is 227.4 sec; & for the MR-111G is 217 sec. We assumed 200 sec Isp for all propulsive maneuvers
Attitude Control	
Control method	3-Axis Wheel-based zero momentum bias with magnetic momentum management
Control reference	Inertial
Attitude control capability	21 arc-seconds – 3 sigma
Attitude knowledge limit	5 arc-seconds – 3 sigma
Agility requirements	Spacecraft is capable of 0.16 degrees/sec maneuver rates (180 degrees in 4.75 minutes)
Articulation/#-axes	3 (2 solar arrays, 1 Ka-band gimballed antenna)
Sensor and actuator information	Each Reaction Wheel has a maximum torque of 0.2 N-m @ 6000 RPM and momentum storage capacity of 100 N-m-s @ 6000 RPM. Spacecraft has six reaction wheels. The gyro's maximum rate for performance is 7 deg/sec with a degraded performance capability up to 300 deg/sec prior to saturation. GPS Receiver: Orbit position knowledge of 0.0025 km 3 sigma and Velocity knowledge of 0.0061 m/sec Each Torque Rod has a capability of 250 A-m^2 linear magnetic moment (spacecraft has three torque rods)
Command & Data Handling	
Spacecraft housekeeping date rate	Average of ∼3.0 kbps
Data storage capacity, Mbits	4,000,000 Mbits/4.0 Tbits at 5 year EOL
Maximum storage record rate	The spacecraft is configured with two LVDS interfaces dedicated for science data operating at 28 MHz with one clock and three data signals. Data rate on each data signal is 7 bits x 28 MHz = 196 Mbps x 3 lines = 588 Mbps for each LVDS interface.
Maximum storage playback rate	The High Speed Science Downlink (Return) link through TDRSS operates at 130.66 Mbps through a Ka-Band Transmitter and 70 watt RF TWTA to a 38 cm diameter antenna. The effective Ka-Band Transmitter symbol rate is 150 Msps
Power	
Type of array structure (rigid, flexible, body mounted, deployed, articulated)	Two deployed, individually articulated solar array wings

Continued on next page

Table 7: Spacecraft Characteristics Table

Spacecraft Component	**Value/Summary, Units**
Array size, meters x meters	Each Solar Array wing consists of three panels with a yoke panel consisting of 2400 Sol Aero 65.2 cm^2 ZTJ solar cells with 6 mil CMG AR/ITO coverglass, BOL efficiency = 28.7%. The solar cells are arranged in 120 parallel strings with 20 cells in series (120P/20S). There are 35 strings on each panel and 15 strings on the yoke. The total area of both solar array wings is 31.3 m^2.
Solar cell type (Si, GaAs, Multijunction GaAs, concentrators)	Sol Aero 65.2cm^2 ZTJ with 6mil CMG AR/ITO cover glass, BOL efficiency = 28.7%
Expected power generation at Beginning of Life (BOL) and End of Life (EOL), watts	11,590 W at 28°C at BOL, 8,360 W at 5 years EOL Our Solar Array is significantly oversized for this mission. We used the existing Landsat 9 Solar Array design (Landsat 9 is a single wing design). We added a second wing, (single axis gimbal and damper) to assure a large power margin. In future development studies of AMEGO we would most likely continue with a two wing design and re-size each Solar Array wing to provide a minimum 30% power margin.
On-orbit average power consumption	Spacecraft: 1,105 W OAP (with 12% contingency included) Instrument: 1,287 W OAP (with 15% contingency included) Observatory (Spacecraft plus Instrument): 2,392 W OAP (with 14% contingency included)
Battery type (NiCd, NiH, Li-ion)	GS Yuasa LSE134 large cell Li-ion
Battery storage capacity, amp-hours	268 A-hr. The spacecraft is configured with two 134 A-hr batteries in parallel.

III.3.2 Spacecraft Technical Maturity

Provide a brief description and an overall assessment of the technical maturity of the spacecraft subsystems and critical components. Provide TRL levels of key units, and in particular, identify any required new technologies or developments or open implementation issues.

No new technologies are needed for the AMEGO spacecraft. A brief description of each subsystem can be found in **Section III.3.1**. **Table 8** describes the TRL level and heritage of each subsystem. A detailed list of spacecraft components can be provided upon request.

III.3.3 Lowest TRL Components

Identify and describe the three lowest TRL units; state the TRL level and explain how and when these units will reach TRL 6. Summarize the TRL of all units less than TRL 4.

See **Table 8** for a description of the TRL of each subsystem. There are no units with TRL less than 6.

III.3.4 Spacecraft Risks

What are the three greatest risks with the spacecraft?

Since there are no new developments anticipated for the spacecraft configuration, the risks are confined to preventing errors in manufacturing, errors in assembly, integration and test and underestimation of the resources required to perform the Statement of Work (SOW).

The greatest risk is underestimating the overall engineering complexity of the observatory, which may have the effect of translating into schedule delays due to the underestimation of the required resources required to perform the work to the agreed to schedule. This can be mitigated by effective use of cost modelling tools in setting aside the necessary funds and developing a realistic schedule to develop the mission in Phase A.

The second greatest risk is preventing errors in component manufacturing, which can lead to spacecraft and observatory schedule erosion. This can be mitigated by selecting component vendors with selection emphasis on past performance (the best track record of delivering components on time) rather than a focus on awarding to the lowest cost bidder.

The third greatest risk is preventing errors in assembly, integration and test. Errors that occur can be mitigated by providing generous funded schedule reserves for the spacecraft integration and test phase and for the observatory integration and test phase. In addition, flight spares or flight repair parts should be procured for each component that has the ability to delay the spacecraft or observatory schedule by more than 90 days if a failure occurs.

III.3.5 Spacecraft Technology Development

If you have required new spacecraft technologies, developments, or if there are open issues, describe the plans to address them (to answer you may point to technology implementation plan reports or concept study reports, but please enumerate the relevant pages.)

There are no required new spacecraft technologies or open issues.

III.3.6 Subsystem Requirements

Describe subsystem characteristics and requirements to the extent possible. Describe in more detail those subsystems that are less mature or have driving requirements for mission success. Such characteristics include: mass, volume, and power; pointing knowledge and accuracy; data rates; and a summary of margins. Comment on how these mass and power numbers relate to existing technology and what light weighting or power reduction is required to achieve your goals.

The observatory mass and power requirements are listed in **Table 6**. The requirements are easily accommodated by standard components that already exist and no light weighting or power reduction is required.

III.3.7 Spacecraft Heritage

Describe the flight heritage of the spacecraft and its subsystems. Indicate items that are to be developed, as well as any existing hardware or design/flight heritage. Discuss the steps needed for space qualification.

The LEOStar-3 product line has extensive heritage, most notably including *Fermi*, which is the same mission class, a very similar operations concept, and similar payload resource needs to

Table 8: Spacecraft Subsystems TRL and Heritage

Subsystem	TRL	Heritage
Structure	6	The overall structure is based on the *Fermi*-LAT spacecraft but since some components need to be reconfigured to meet AMEGO instrument and mission requirement we conservatively assume TRL 6.
RF Comm	6	Ka antenna being used for the European MetOP SG mission (>12 antennas) Identical Ka TWTAs will be flown on JPSS-2. These units are in the same family of TWTA units produced for *Kepler*, *LRO* and NASA Connect. An identical Ka Modulator will be flown on JPSS-2. This unit is highly similar to the T-737 design with digital filtering and modulation at a 1.5 GHz IF vs. the T-737 which implemented direct X-Band analog modulation. The T-737 was specifically built for the JPSS-1 (2017) mission. Identical gimbal will be flown on JPSS-2 (2020). Similar (Type 5) Gimbals were flown on *XTE* as a 2 axis antenna pointing mechanism. The Gimbal Drive Electronics were flown on the *Lunar Reconnaissance Orbiter (LRO)*. Modifications will be made to the unit's waveguides which brings the unit's TRL to 7 S-band transceiver being used on Cygnus vehicles CRS-1&2 and LandSAT-9 We conservatively estimate TRL 6 due to the need for a custom harness.
Thermal	9	Standard temperature sensors, heaters, and MLI.
Power	7	PDU has heritage from *Swift*, *Fermi*, *Landsat 8* and *ICESat-2*. The thermal interface boards are a new development for Landsat 9 and are currently TRL 8 (passed environmental test at the PDU component level). The Moog Type 5 Solar Array Drive has been flown on *Fermi*, *Swift* and *Landsat 8*. The battery has heritage on *ICESat-2*, Landsat 9 and JPSS-2. The solar array is similar to *Landsat 8* with configuration alterations necessary to meet AMEGO requirements.
ADCS	8	All components have flight heritage on Northrop Grumman satellites Over 700 similar reaction wheels units have flown, including on *Landsat 8*. The IMU has flown on numerous GEOStar-2* spacecraft and on OCO-2. Sun Sensors flew on *SORCE*, *GALEX*, *AIM*, *Dawn*, *NuSTAR* and *OCO-2*. Zarm Technik has flown numerous magnetometers, including on *ICESat-2* and Landsat 9. GPS receiver identical to Landsat 9 and JPSS-2 (qualified in 2017).
C&DH	7	LEOStar-3 IEMs flown on *Swift*, *Fermi*, *Landsat 8*, *ICESat-2* (2017) and JPSS-2 (2020). Most cards are TRL 9 with the exception of the Spacewire and Memory cards. Similar Spacewire and Memory cards are being developed on JPSS-2 (2020. The solid state recorder proposed for AMEGO is based on the Landsat 9 design with minor design changes.
Propulsion	7	Propellant tank, 22N thruster, 5N thruster, latch valves, pressure transducers are identical to *ICESat-2*, *Landsat 8* and Landsat 9. All propulsion tubing and harness designs are custom.

AMEGO. The AMEGO spacecraft is a fully redundant LEOStar-3, which will make extensive use of existing mechanical and thermal designs from the *Fermi* spacecraft. There are no items that are to be developed or need space qualification.

III.3.8 Instrument/Spacecraft Accommodation

Address to the extent possible the accommodation of the science instruments by the spacecraft. In particular, identify any challenging or non-standard requirements (i.e. Jitter/momentum considerations, thermal environment/temperature limits etc.).

The instrument is mounted externally to the spacecraft via a set of titanium flexures. There are no challenging requirements on the spacecraft.

III.3.9 Spacecraft Schedule

Provide a schedule for the spacecraft, indicate the organization responsible and describe briefly past experience with similar spacecraft buses.

In the baseline mission described here, the spacecraft is provided by Northrop Grumman. The AMEGO mission schedule provides 52 months from the start of spacecraft assembly to mission launch. See **Section VI.3 for more details**.

III.3.10 Spacecraft Non-US Participation

Describe any instrumentation or spacecraft hardware that requires non-US participation for mission success.

No non-US participation is required.

III.3.11 Spacecraft Special Requirements

Provide any special requirements such as contamination control or electromagnetic controls (EMC).

There are no spacecraft special requirements.

IV Enabling Technology

Please provide information describing new Enabling Technologies that must be developed for activity success.

There are no new enabling technologies that need to be developed for AMEGO.

IV.1 Technology Maturation Plan

For any technologies that have not been demonstrated by sub-scale or full-scale models, please provide a description of the technical maturity, including the description of analysis or hardware development activities to date, and the associated technology maturation plan.

N/A

IV.2 Technologies Critical to Mission Success

Describe the aspect of the enabling technology that is critical to the mission's success, and the sensitivity of mission performance if the technology is not realized or is only partially realized.

N/A

IV.3 Cost and Schedule Assumptions

Provide specific cost and schedule assumptions by year for all developmental activities, and the specific efforts that allow the technology to be ready when required, as well as an outline of readiness tests to confirm technical readiness level.

N/A

IV.4 Non-US Technology

Please indicate any non-US technology that is required for mission success and what back up plans would be required if only US participation occurred.

N/A

V Mission Operations Development

Please answer the following, or point to pages in existing public documentation where the information is provided:

V.1 Operational Complexity

Provide a brief description of mission operations, aimed at communicating the overall complexity of the ground operations (frequency of contacts, reorientations, complexity of mission planning, etc.). Analogies with currently operating or recent missions are helpful. If the NASA DSN network will be used, provide time required per week as well as the number of weeks (timeline) required for the mission.

The AMEGO ground system uses existing facilities and systems to provide reliable low cost and low risk operations (**Figure 25, Table 9**). The Space Network (SN) provides the primary space to ground link. Near Earth Network (NEN) ground stations in Singapore, Hawaii, and Malindi provide backup to the SN for housekeeping telemetry and commanding. For normal operations, AMEGO has a 5 min TDRSS contact every orbit to provide for low latency. With the Ka-band downlink capability of 150 Mb/sec, this provides 45% margin allowing for occasional missed contacts andor temporary increases in data volume from solar flares etc. The spacecraft has storage for over 24 hours of data, so if there are problems with the contacts or in scheduling contacts, data are not lost as long as the problems are resolved within a day.

The Virtual Multi-Mission Operation Center (VMMOC) provides the operation of the observatory. The VMMOC provides existing capabilities and infrastructure, including a secure and reliable facility, and an existing team of operations staff and supporting services such as IT security and systems administration. It is currently supporting *Fermi* (a probe-scale mission with very similar operations concept), as well as *ACE* and *WIND*. The VMMOC provides: telemetry and command processing using the Integration and Test Operations System (ITOS), which has been used to support in-house spacecraft for over 25 years; mission planning, including ground station scheduling and command load generation for the spacecraft and instruments; trend analysis to monitor flight system performance; orbit determination using the General Mission Analysis Tool; post-launch attitude sensor calibration; and automated monitoring when VMMOC is unstaffed.

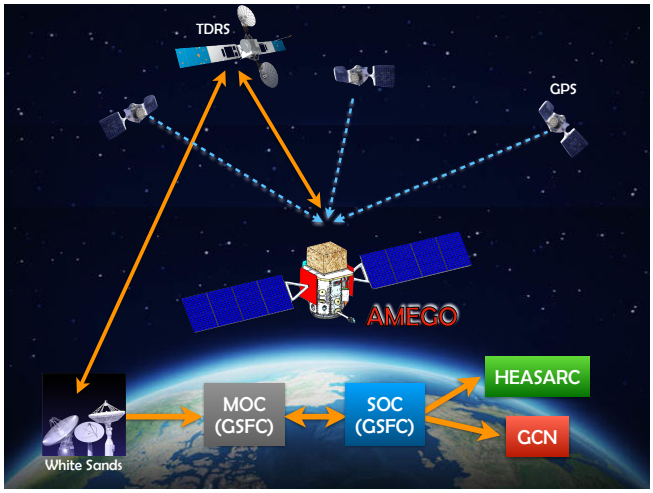

Figure 25: AMEGO communication, data, and commanding paths through space network and ground systems.

The Flight Operations Team (FOT) at the VMMOC is responsible for the operation, health, and safety of the observatory. The observatory is commanded via weekly command loads. The Science Operations Center (SOC) provides weekly commanding inputs to the FOT, which generates and checks the command sequence prior to uplinking to the spacecraft. Based on the planned orientations, the FOT models the expected visibility of communication satellites and schedules the TDRSS contacts used for commanding and science data/telemetry downlinks. While the VMMOC is staffed only during business hours for normal operations, one member of the FOT is always on call to respond rapidly to unexpected circumstances. Ground system automation checks telemetry from every downlink and alerts on-call personnel if the monitored values exceed defined limits, if telemetry is interrupted, if an unplanned spacecraft event occurs, or if other situations arise requiring attention.

The SOC is also located at GSFC. It receives the level zero processed data from the VMMOC and processes them autonomously into higher level data products, including transient alerts. The SOC software is based on existing software and will include some new algorithms for processing the Compton scattering measurements.

Table 9: Mission Operations and Ground Data Systems Table

Downlink Information	**Values**
Number of contacts per day	15 Ka band contacts
Downlink Frequency Band	S-band: 2.2475 GHz, Ka-band 26.7034 GHz
Telemetry Data Rate(s)	S-band: 13, 948 bps (data) 32,000 bps (fully encoded symbol rate) Ka-Band: 130,664,063 bps (data) 150,000,000 Bps (fully encoded symbol rate)
Spacecraft Transmitting Antenna Type(s) and Gain(s)	The spacecraft is configured with an S-band command and telemetry link using two hemispherical coverage antennas that are linked to a 10 watt RF power S-Band Transceiver through a 3dB coupler. The hemispherical coverage antenna has a transmit gain of 2.7 dBi The science downlink is configured with a Ka-Band transmitter coupled to a 70 watt (RF) Travelling Wave Tube Amplifier (TWTA) into Cassegrain High Gain Antenna (HGA) measuring 39.5 cm diameter with a transmit gain of 37 dBi. The spacecraft has a two-axis gimbal which auto-tracks TDRSS
Spacecraft Transmitter peak power	Spacecraft S-Band Transmitter 10 watts RF output (built-in Solid State Power Amplifier). Spacecraft Ka-Band Transmitter output is selectable from -10 to +10 dBm in 0.5 & 1 dB steps.
Downlink Receiving Antenna gain	TDRSS
Transmitting Power Amplifier Output	Ka-Band Travelling Wave Tube Amplifier (TWTA) 70 W RF power
Uplink Information	
Number of Uplinks per day	1
Uplink Frequency	S-Band: 2.06727 GHz
Telecommand Data Rate	S-band: 16,000 sps
S/C receiving antenna type(s) and gain(s)	The S-Band hemispherical coverage antenna has a receive gain 3.5 dBi for $>90^{\circ}$ coverage

V.2 Unusual Ground System Constraints

Identify any unusual constraints or special communications, tracking, or near real-time ground support requirements.

There are no unusual constraints or other needs.

V.3 Challenging Operational Constraints

Identify any unusual or especially challenging operational constraints (i.e. viewing or pointing requirements).

There are no unusual or especially challenging operational requirements.

V.4 Science Data Products

Describe science and data products in sufficient detail that Phase E costs can be understood compared to the level of effort described in this section.

V.5 Science and Operations Center

Describe the science and operations center for the activity. Will an existing center be expected to operate this activity? How many distinct investigations will use the facility? Will there be a guest observer program? Will investigators be funded directly by the activity?

The Science Operations Center (SOC) will be located at Goddard Space Flight Center. The role of the SOC will be to provide the scientific community with data, science analysis tools, and documentation as well as manage a Guest Investigator (GI) program, where investigators will be funded directly. Members of the SOC will create an observing timeline based on the default observing mode and any successful GI observing proposals. The data telemetered down from the instrument enters the ground system through the Virtual Multi-Mission Operation Center (VMMOC), staffed by the Flight Operations Team (FOT) which will also be housed at GSFC, as it is for the *Fermi Observatory*. The SOC receives telemetry from the VMMOC, monitors the instrument subsystems through the housekeeping portion of the telemetry, process the science data, and transmits the resulting science data products to the instrument teams and the public. The science data processing is well understood and will have similar scope and complexity to data processing from the *Fermi*-LAT, starting with event reconstruction from the 'hits' in different parts of the instrument and ending with a characterization of these events. This will be hosted at GSFC and aided by the expertise at Space Sciences Laboratory (SSL) at Berkeley. Data processing levels are described in **Section III.1.8**. NASA/GSFC has experience with hosting large data-sets such as those hosted by HEASARC and the NASA Earth data archive. GSFC has been the data archive and science support center for all NASA large-scale gamma-ray missions.

V.6 Data Archive

Will the activity need and support a data archive?

The data archive model will be similar to *Fermi* and will be co-hosted at HEASARC at NASA/GSFC.

VI Programmatics and Schedule

Please answer the following, or point to pages in existing public documentation where the information is provided:

VI.1 Organizational Chart

Provide an organizational chart showing how key members and organizations will work together to implement the program.

Figure 26 lists the AMEGO organizational chart describing the structure and flow of institutional responsibilities.

VI.2 Risk Chart

Provide a table and a 5x5 risk chart of the top 3 risks to the program. Briefly describe how each of these risks will be mitigated and the impact if they are not. (Mass, power, schedule, cost, science, etc.).

Figure 27 illustrates the top 3 risks to the program, which are described in detail in **Section III.1.3**.

VI.3 Phase Schedule

Provide an overall (Phase A through Phase F) schedule highlighting key design reviews, the critical path and the development time for delivery required for each instrument, the spacecraft, development of ground and mission/science operations etc. Include critical on-orbit events such as maneuvers, instrument deployments, etc.

The top-level overall schedule (**Figure 29**) is developed to mitigate risk and includes appropriate reserve for a probe class mission. During Phase A we will build a tracker Segment Structure Mass Model (SSMM) and a tracker Segment Engineering Model (SEM). The SSMM consists of two tracker segments (the carbon rib structure and 16 dummy detectors that simulate the Si DSSDs). This will be used to mitigate the risk due to the mechanical structure (**Section III.1.3**, Risk 4). The schedule includes enough time to design and test the structure. Concurrently, we will build a SEM (two segments) which will be used to verify our tracker assembly method (including the wire bonding) and thoroughly test the tracker segment to verify that it meets requirements (scientific, technical, and thermal). This also verifies that the DSSD vendor can deliver to specifica-

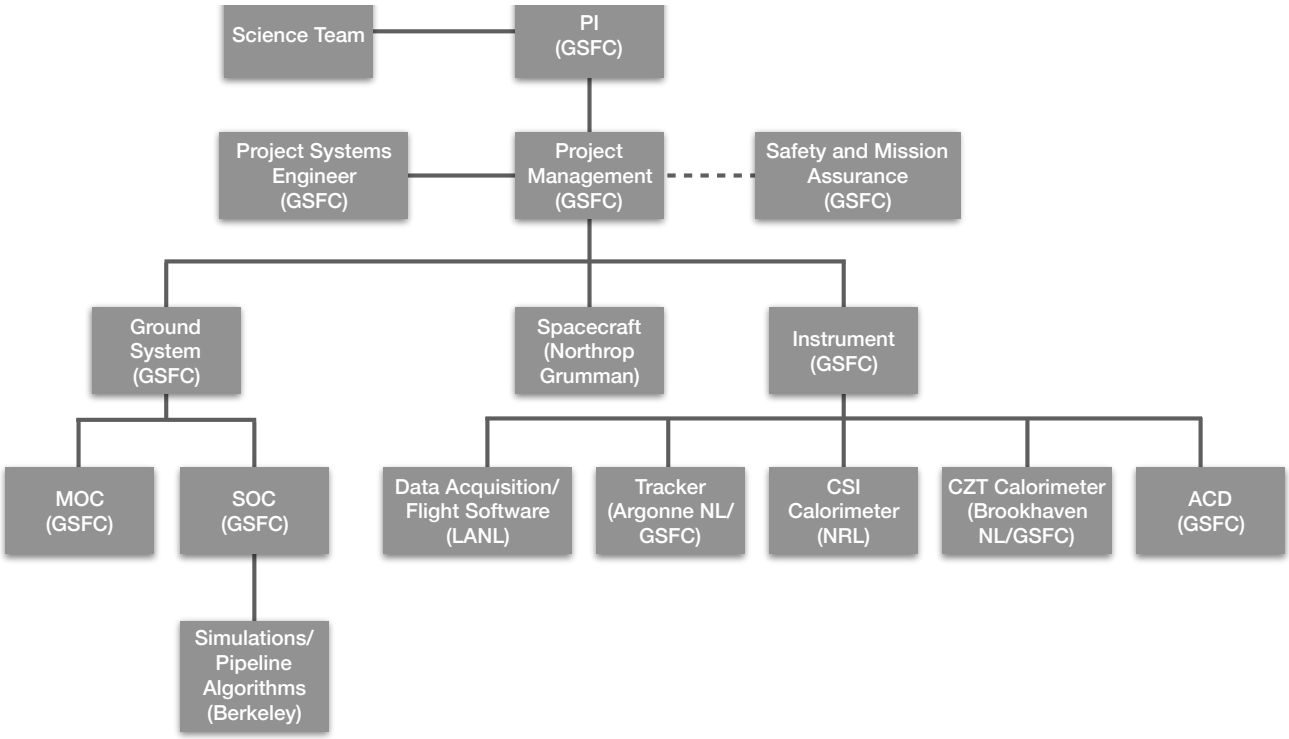

Figure 26: AMEGO Organizational Chart

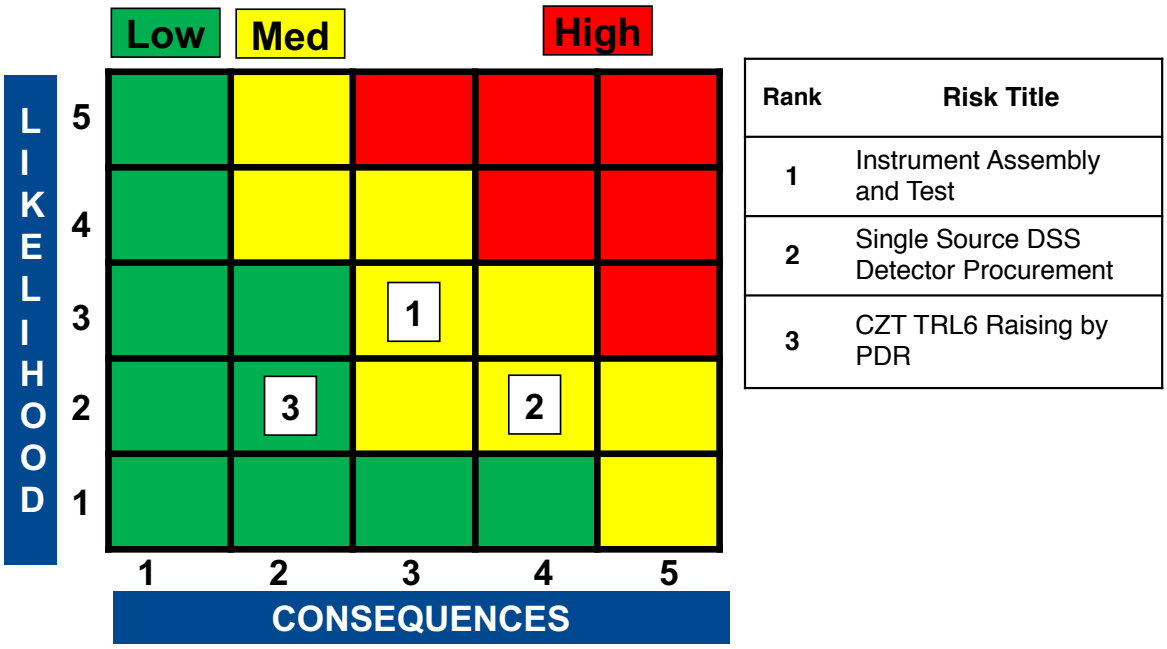

Rank	Risk Title
1	Instrument Assembly and Test
2	Single Source DSS Detector Procurement
3	CZT TRL6 Raising by PDR

Figure 27: Top 3 risks to the AMEGO program.

tions and on time. During this time we will also build a CZT low energy calorimeter Array Structure Mass Model (ASMM) and Array Engineering Model (AEM). The ASMM will be a single array of CZT modules (50 modules of 4 x 4 dummy detectors) to verify the mechanical design and mitigate Risk 3. The AEM will be four 4x4 CZT modules to verify the electrical design and show that it meets requirements. This will also allow us to verify that the CZT vendor can deliver to specifications and schedule. All of these activities will end prior to the Science Requirements Review (SRR) which occurs several months prior to the end of Phase A. **Figure 28** provides an overview of the various test units that will be developed and tested.

Phase B begins after Key Decision Point (KDP) B (6 months after the end of Phase A). The final designs of the tracker and the two calorimeters occur during this phase and we build a full Tower Structure Mass Model (TSMM). The other three towers will be simulated via simple mass models that do not include internal structures to simulate the presence of the other towers. The TSMM will incorporate a full tower of 60 segments (the top two layers will have dummy detectors that simulate the DSSDs) and four full Low-Energy Calorimeter arrays (populated with dummy detectors). A High-Energy CsI Calorimeter mass model is also constructed during this time. The first 3 months of the year-long phase B will be devoted to design work, and the next 8 months will be building and testing the mass models. The TSMM will be built in four parallel lines so that it can be fully completed and tested prior to PDR and the end of Phase B (so as to raise the TRL of all subsystems to 6 prior to PDR). The building and assembly of the TSMM will not only verify the structure of the tracker and calorimeters but also validate our assembly line. To complete these tasks within Phase B, some long-lead procurements and design work will begin prior to KDP B, but no funds will be committed (see **Figure 30** for an example).

Phase C begins after KDP C and a few weeks after PDR. We will start the procurement process of the ASICs (for both the tracker and the Low-Energy calorimeter), the DSSDs, and the CZT during Phase B so that the first deliveries of the ASICs, CZT, and DSSDs occur soon after the beginning of Phase C. There is approximately 9 months between the last deliveries for the SEM and AEM and the start of the procurement process; giving time to work with the vendor if issues are seen with the SEM and/or AEM detectors or ASICs. There is also 9 months between the awarding of the contract and the first deliveries of the ASICs, DSSDs, and CZT. The vendors have confirmed that they can deliver the first batches of ASICs and detectors in this time frame.

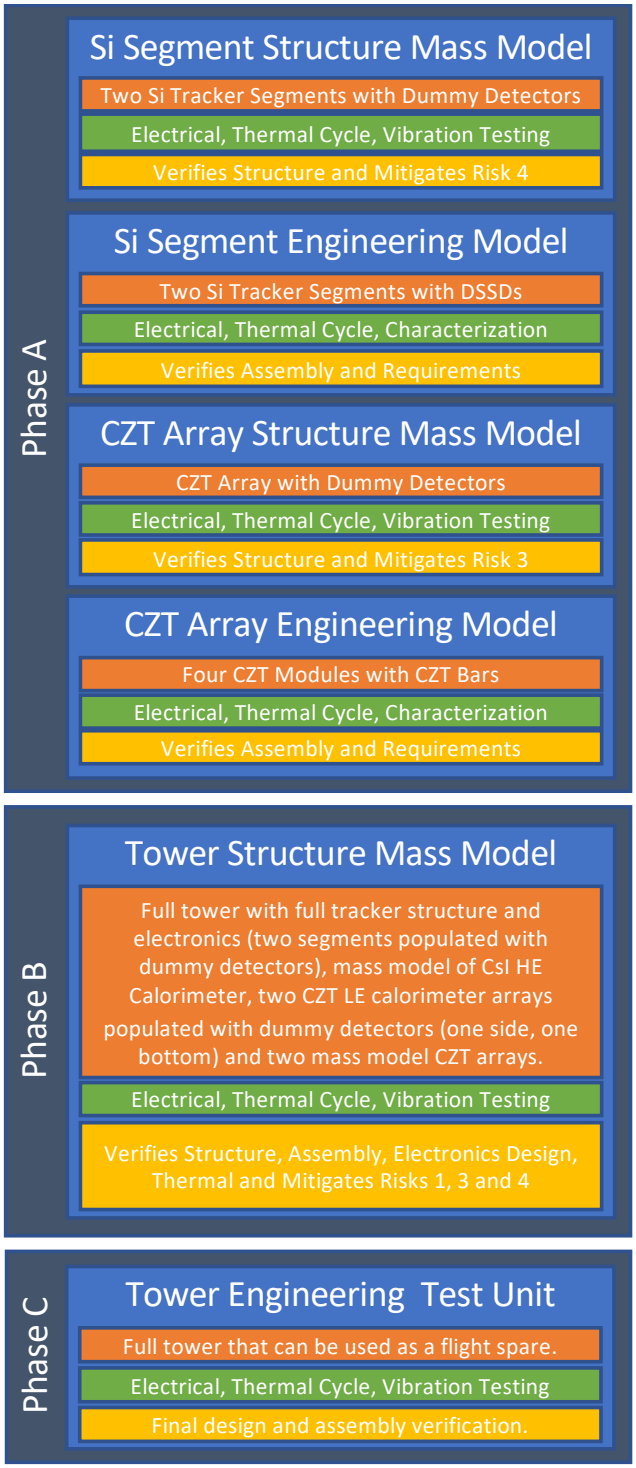

Figure 28: Test units are designed, integrated and tested during different phases to verify the design, assembly, and requirements as well as to reduce risk. The work in Phase A and B raises the TRL of any low-TRL subsystems to TRL 6. In each panel, the description of the test unit is shown in the first block (orange), the tests are shown in the second (green) and the result is shown in the last block (yellow).

ASICs and detectors are delivered in batches. The CZT will be delivered monthly over the course of 2.4 years and the DSSDs over the course of two years. To reduce risk, a single tower Engineering Test Unit (ETU) of the Tracker, single tower ETU CsI calorimeter, and four ETU CZT arrays (enough for a single tower) will be built immediately after PDR in Phase C. This ETU will be used to verify the final design and verify the requirements. During the ETU build, each segment of the tracker and each CZT array will undergo a thermal cycle and a limited performance test to draw down risk (since it will be difficult to remove segments post-integration, it is critical to confirm that each segment is functional prior to insertion in a tower). The CZT, CsI and Tracker will be integrated into a full ETU tower (along with mass simulators of the other towers) and undergo full electrical, functional, and environmental tests. The ETUs can be used as flight spares of the flight towers. The successful completion of these tests will lead to CDR. Note that the tracker segments and CZT modules are built serially. We have the capacity for multiple assembly lines in case of schedule overruns, so the current schedule can be considered a conservative effort. As detectors arrive (CZT and Si) they are assembled into segments or modules. These segments are delivered to the tower assembly (for the tracker) or the CZT array assembly (for the Low-Energy Calorimeter) and these assemblies and testing happen in parallel to the individual segment and module assembly.

Post CDR, the assembly of the flight segments and modules commences. The segments are built and tested in batches of 5. The final segment delivery occurs in April 2026 (with the tower assembly occurring shortly thereafter) and the final array delivery is in early April 2026. Following this there is 45 (working days) funded schedule reserve for both the CZT and the Tracker. The CZT arrays are delivered first to integrate with the CsI calorimeter (delivered from NRL in late April 2026). Note that we can deliver the first 8 CZT arrays earlier for early integration with the CsI calorimeter if needed. The final 8 arrays are not needed until final integration. This full assembly is then integrated and tested until December 31, 2026. We have included 4 calendar months of funded schedule reserve post instrument I & T. A systems integration review is scheduled prior to shipment to the vendor for observatory I & T.

A detailed schedule for the High-Energy Calorimeter is not included; it is a simplified version of the *Fermi*-LAT calorimeter, and the development, integration and test schedule is not aggressive compared to the LAT schedule. Phase C also includes development of the MEM, ACD, and MMS.

The spacecraft development takes 52 calendar months based on the the LEOStar-3 development cycle (including all spacecraft and observatory integration and test). This development will begin immediately post CDR. The observatory will be integrated after KDP D, which starts Phase D. Observatory integration will take 6 months, be capped off with a pre-environmental review and followed by environmental testing. Four months of funded schedule reserve follows observatory I & T.

Ground systems development begins post-CDR, and the development of the mission operations system starts alongside instrument I & T and continues though the end of Phase E. Phase E is baselined as 5 years and ends at KDP F. 3 months of closeout (Phase F) is included.

The critical path is though the delivery of the DSSDs and assembly and test of the tracker (shown as a red line in **Figure 29** and in more detail in **Figure 30**). We have included sufficient funded schedule reserve (2.25 months in tracker assembly and 4.25 months post instrument I & T resulting in 1.5 months of reserve per year) to mitigate against delays along the critical path. The DSSDs final delivery is approximately a year prior to the assembly of the final segment so some delivery delays can be accommodated into the schedule. If delays are encountered during segment assembly, we can implement an additional assembly line (Argonne has the capacity for up to two parallel lines).

VI.4 Non-US Contributions

Provide a description of any foreign contributions and their extent.

N/A

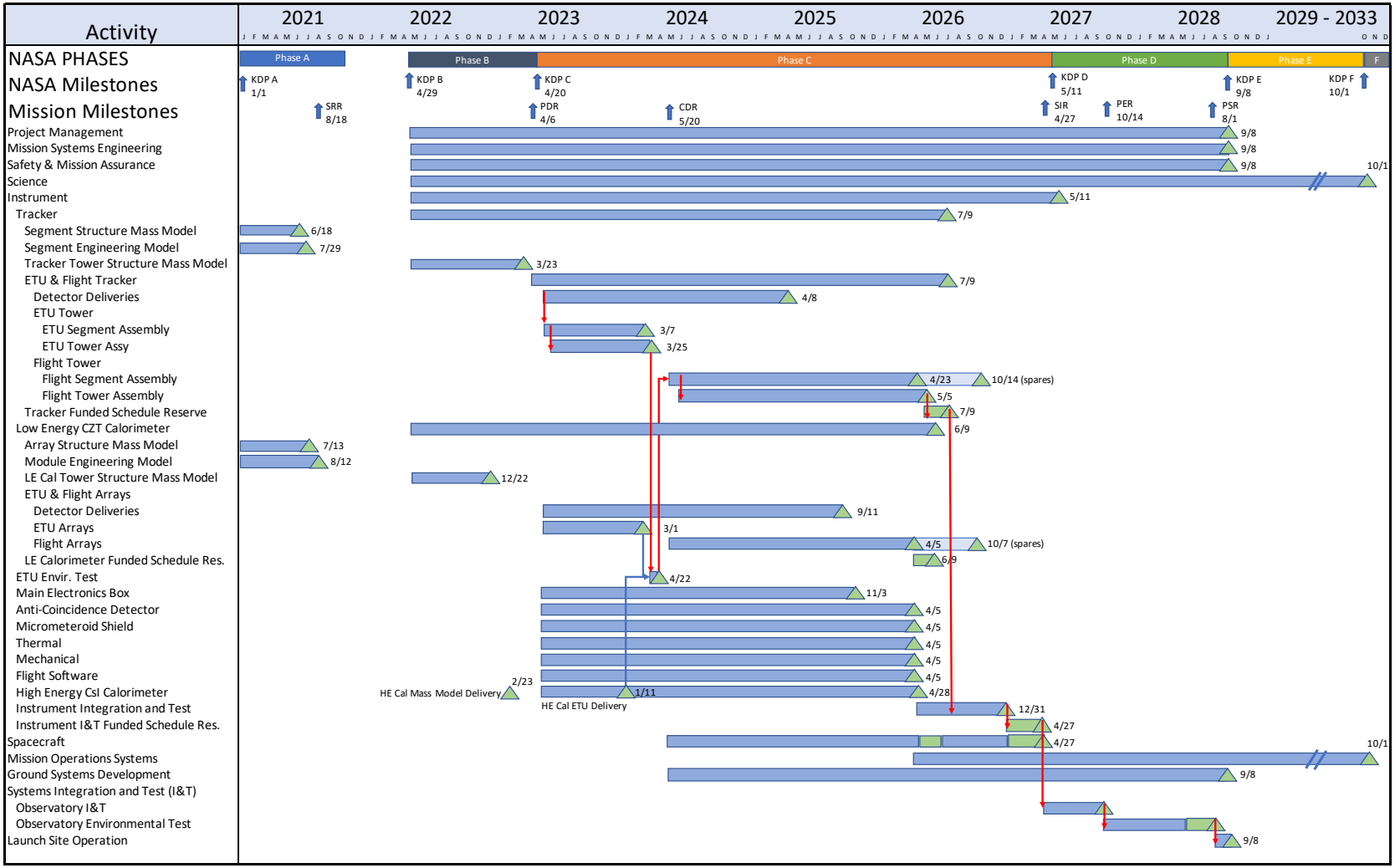

Figure 29: The top level schedule is designed to mitigate risk and incorporates sufficient reserve. The major mission milestones are scheduled at specific points in time to verify progress: the Science Requirements Review occurs at the end of the testing of the mass models and engineering models of the tracker and Low-Energy Calorimeter; PDR occurs after the environmental testing of the full tower mass model; and CDR occurs after the assembly and test of the full tower ETU. The deliveries of the DSSDs and CZT bars occur in batches over several years. The critical path is through the tracker assembly and is indicated by the red arrows. Sufficient funded schedule slack is included and is appropriate for a probe scale mission.

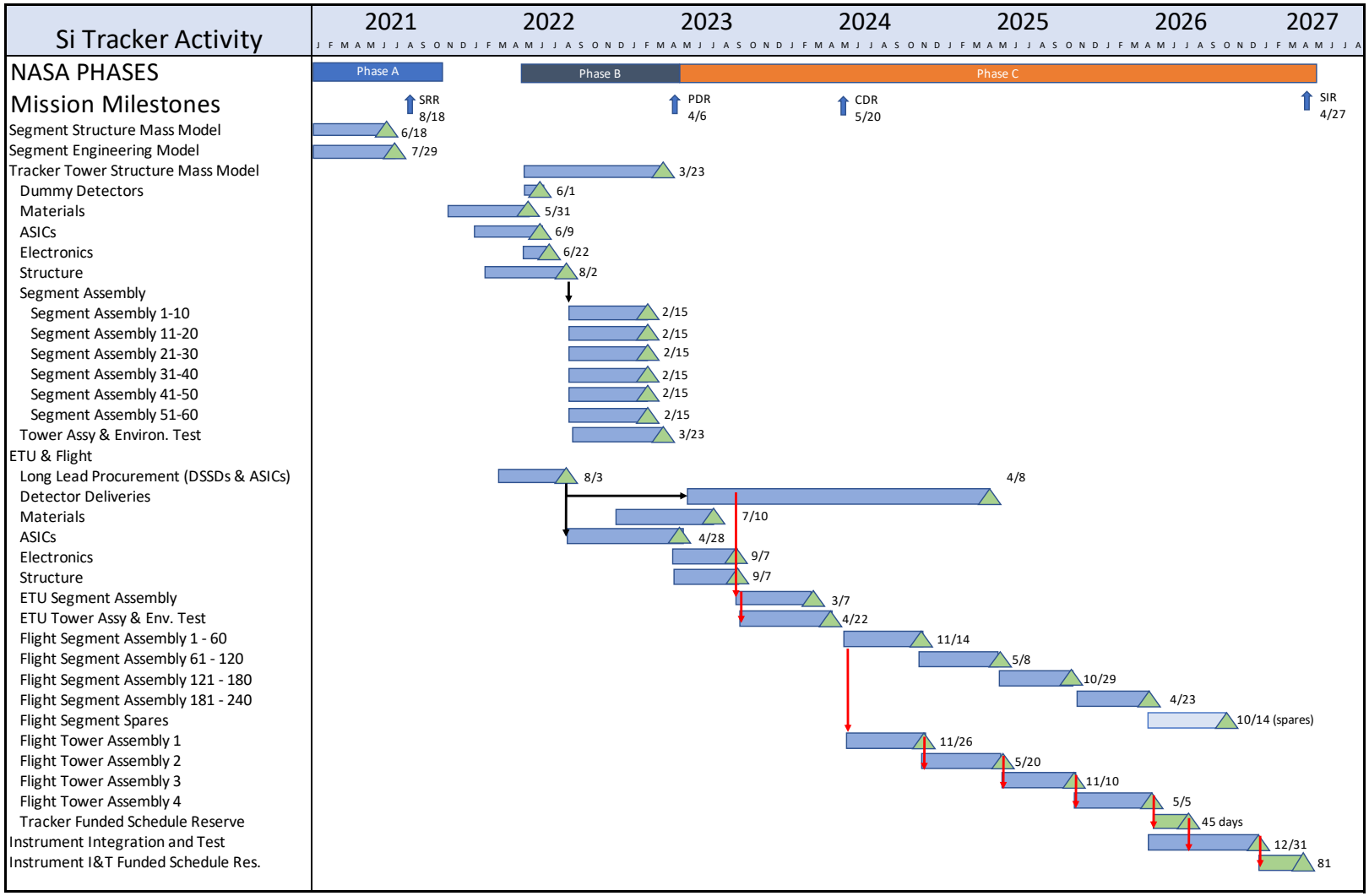

Figure 30: The critical path is through the tracker DSSD deliveries, segment assembly, and tracker tower assembly. The risk of the critical path delaying the overall schedule is mitigated by the inclusion of funded schedule reserve, building enough spare segments to build another tower, and starting the procurement process for long-lead items prior to the start of Phase B. Additionally, the ETU that is built early in Phase C prior to CDR can be used as a flight tower. Shown here is the detailed tracker schedule that highlights the critical path as red arrows.

VII Cost

Please answer the following, or point to pages in existing public documentation where the information is provided:

VII.1 FTE Estimates and Cost by Year/Phase

Provide FTE estimates and cost by year/Phase for all expected science personnel.

Table 10 provides estimated costs per mission element.

VII.2 Foreign Partners

If a foreign agency is assumed to be a partner or a major contributor, provide an estimate by year and Phase for the cost breakdown between NASA and any foreign contributions. This should be separate, but consistent with Total Mission Cost Funding Table.

VII.3 Phase A

Provide a description and cost of what will be performed during Phase A by year. Also include total length of Phase A in months and total Phase A estimated costs.

Figure 28 details the test units that will be built and tested during Phase A (we build and test the SSMM, SEM, ASMM, and AEM). We chose to perform these specific tasks to reduce the likelihood of two of the top 3 risks to the mission (1 and 3, **Figure 27** and **Section III.1.3**). Risk 2 is also somewhat mitigated by the development of the SEM (it verifies the production line at the vendor and performance of the DSSDs). The science requirements will be developed and refined and the results of the testing of the mass and engineering models will feedback into this process. The SRR occurs several months prior to the end of Phase A. Post-SRR Phase A activities include refining the system architecture, developing the procurement strategy for the DSSDs and CZT bars, and drafting the requirements verification plan. A detailed schedule, WBS structure, and costing will be performed. Although not specifically occurring during Phase A, some activities are begun between Phase A and B to mitigate delivery delays. These include beginning the procurement process for long lead items such as the composite materials, DSSDs, ASICs, and CZT. We have structured Phase A and chosen activities that provide the most impact to reducing risk and schedule delays while judiciously using the funds available to the project during this time. Phase A lasts 10.4 calendar months and the activities planned are scaled up versions of those planned for the ComPair MidEx proposal and thus the cost of Phase A is appropriate for a Probe Class mission like AMEGO.

VII.4 Mission Cost Funding Profile

Please fill out the Mission Cost Funding Profile table assuming that the mission is totally funded by NASA and all significant work is performed in the US.

An engineering design study for a similar mission concept was performed by a Goddard team in 2016. This mission had the same physical footprint, but fewer Silicon and CsI layers than AMEGO and did not have a CZT calorimeter. Cost estimates for this mission study were established with the CEMA/price-H and RAO teams at Goddard.

The cost of AMEGO was established by scaling the price-H costs of the tracker and CsI calorimeter from the 2016 study and adding a bottoms up cost estimate for the CZT calorimeter based on vendor quotes, detailed schedule and realistic labor needs. Note that both AMEGO and the prior mission assume redundancy through graceful degradation so the instrument costing for the prior MidEx mission is appropriate for the rendundancy requirements for a probe in this case (similar to *Fermi*). Estimated spacecraft costs are also derived from the 2016 study using the upper end of the estimates from the price-H costing team at Goddard (note that this is more than a factor of two more expensive than the actual spacecraft cost for *Fermi*). The launch services assume a Falcon 9 launch to a low earth orbit. The science cost covers development and operation of a science data center and a 5-year Guest Investigator program. The mission and Instrument Operations include development of the mission and science operations centers, observatory operations, and instrument data processing from level 0 to level 4. The costs for the other mission elements are estimates derived by assuming average fractional mission costs for medium-sized missions.

In this cost estimate, we assume that all support for AMEGO is from US Federal funds. However, we note that the expectation is that international contributions will provide a significant fraction of the

payload.

The conclusion is that AMEGO comfortably fits in the Medium (Probe) cost category at ∼$784M ($1019M including 30% contingency).

The majority of the payload costs will be utilized during Phase C through SIR. Some payload costs will be expended in Phase B to produce the preliminary design and develop the ASMM and TSMM. Spacecraft costs will be incurred starting with CDR in Phase C and continuing on through Phase D. Project Management, Systems Engineering, Science, and Safety & Mission Assurance costs are relatively even throughout the project through the end of Phase D (some costs are incurred in Phase A, see **Section VII.3**). The ground system WBS starts in Phase C post CDR and continues through the end of Phase E (some of the cost is to develop mission operations and some for the ground system). Systems I&T costs are exclusively used during Phase D. Based on this we plan on spending $5M, $53M, $372M, $242M, and $112M in phases A - E respectively (margin is not included in these numbers).

VII.5 Second Mission Cost Funding Profile

For those partnering with foreign or other organizations, provide a second Mission Cost Funding Profile table, Table 5, and indicate the total mission costs clearly indicating the assumed NASA and contributed costs.

Table 10: *Estimated costs per mission element.*

WBS	Cost ($M)	Notes
Project Management	45	6%
Systems Engineering	45	6%
Safety and Mission Assurance	36	5%
Science	86	Includes science data center and 5-year GI program
Payload	170	Scaled instrument costs from 2016 study with additional bottoms-up estimate for CZT calorimeter
Spacecraft	150	Based on recent parametric estimates for similar spacecraft
Mission Operations	80	10%
Launch Services	100	Based on DSCOVR Falcon 9 launch costs
Ground Systems	36	5%
Systems Integration and Test	36	5%
Total	**784**	
Total with 30% margin	**1019**	

Acronym List

ACD - Anti-coincidence detector
ACDS - Attitude Determination and Control Sub-system
ADU - Analog-Digital Unit
AD - Analog-Digital
AEM - Array Engineering Model
AG - Active Galactic Nuclei
AMEGO - All-sky Medium Energy Gamma-ray Observatory
AMS - Alpha Magnetic Spectrometer
APRA - Astrophysics Research and Analysis
ARM - Angular resolution measure
ASIC - Application specific integrated circuit
ASMM - Array Structure Mass Model
BCP - Ball Commercial Platform
C&DH - Command and Data Handling
CAD - Computer Aided Design
CALET - CALorimetric Electron Telescope
CBE - Current Best Estimate
CDR - Critical Design Review
CGRO - Compton Gamma-Ray Observatory
CGRO-COMPTEL - CGRO-Imaging Compton Telecope
CGRO-EGRET - CGRO-Energetic Gamma Ray Experiment Telescope
CFRP - Carbon Fiber Reinforced Polymers
COSI - Compton Spectrometer and Imager
COTS - Commercially off the shelf
CPU - Central Processing Unit
CsI(Tl) - Thallium doped Cesium Iodide
CZT - Cadmium Zinc Telluride
DSSDs - Double-sided silicon detectors
EPS - Electrical Power Subsystem
ETU - Engineering Technical Unit
eXTP - enhanced X-ray Timing and Polarimetry mission
Fermi-GBM - *Fermi*-Gamma-ray Burst Monitor
Fermi-LAT - *Fermi*-Large Area Telescope
FEE - Front end electronics
FEM -
FITS - Flexible Image Transport System
FOT - Flight Operations Team
FOV - Field of view
FSW - Flight Software
FWHM - Full width half maximum
GEVS - General Environmental Verification Specification
GRB - Gamma-ray burst
GSFC - Goddard Space Flight Center
HEAO - High Energy Astronomy Observatory
HVPS - High-voltage power supply
IDEAS - Integrated Detector Electronics AS
IEM - Intergrated Electronics Module

INTEGRAL - INTErnational Gamma-Ray Astrophysics Laboratory
INTEGRAL-SPI - Spectrometer on-board INTEGRAL
ITOS - Integration and Test Operations System
KDP - Key decision point
KSC - Kennedy Space Center
LEO - Low Earth orbit
MEGA - Medium Energy Gamma-ray Astronomy telescope
MEGAlib - Medium Energy Gamma-ray Astronomy library
MEM - Main electronics module
MIDEX - Medium-Class Explorer
MLI - Multi-layer insulation
MMS - Micro Meteoroid Shield
NRL - Naval Research Laboratory
NuSTAR - Nuclear Spectroscopic Telescope Array
OAP - Orbit Averaged Power
OCXO - Oven-controlled crystal oscillator
PAMELA - Payload for Antimatter Matter Exploration and Light-nuclei Astrophysics
PCB - Printed circuit board
PDR - Preliminary Design Review
PER - Pre-Environmental Review
PIE - Payload Interface Electronics
PMT - Photomultiplier tubes
PSF - Point spread function
PSR - Pre-Ship Review
QED - Quantum electrodynamics
RAAN - Right ascension of the ascending node
RSDO - Rapid Spacecraft Development Office
RHESSI - Reuven Ramaty High Energy Solar Spectroscopic Imager
RTW - Real-Time Workshop
SAA - South Atlantic Anomaly
SADA - Solar Array Drive Assembly
SEM - Segment Engineering Model
SiPM - Silicon photomultipliers
SIR - System Integration Review
SIRI - Strontium Iodide Radiation Instrumentation II
SIRU - Scalable Inertial Reference Unit
SN - Supernova
SRR - Science Requirements Review
SSMM - Segment Structure Mass Model
SSR - Solid State Recorder
STM - Science Traceability Matrix
TAM - Three Axis Magnetometer
TDRSS - Tracking and Data Relay Satellite System
TRL - Technology Readiness Level
TSMM - Tower Structure Mass Model
VMMOC - Virtual Multi-Mission Operation Center
WLS - Wave-length shifting bars

References

[1] Eric Burns, A. Tohuvavohu, J. M. Bellovary, et al. Opportunities for Multimessenger Astronomy in the 2020s. *Astro2020 White Paper*, 51(3):250, May 2019.

[2] Eric Burns, S. Zhu, C. M. Hui, et al. Gamma Rays and Gravitational Waves. *Astro2020 White Paper*, 51(3):260, May 2019.

[3] Eric Burns, Aaron Tohuvavohu, James Buckley, et al. A Summary of Multimessenger Science with Neutron Star Mergers. *Astro2020 White Paper*, 51(3):38, May 2019.

[4] Tonia Venters, Kenji Hamaguchi, Terri J. Brandt, et al. Energetic Particles of Cosmic Accelerators I: Galactic Accelerators. *Astro2020 White Paper*, 51(3):396, May 2019.

[5] Zorawar Wadiasingh, George Younes, Matthew G. Baring, et al. Magnetars as Astrophysical Laboratories of Extreme Quantum Electrodynamics: The Case for a Compton Telescope. *Astro2020 White Paper*, 51(3):292, May 2019.

[6] Mattia Di Mauro, Silvia Manconi, and Fiorenza Donato. Prospects for the detection of synchrotron halos around middle-age pulsars. *Astro2020 White Paper*, 51(3):183, May 2019.

[7] Frank Timmes, Chris Fryer, Frank Timmes, et al. Catching Element Formation In The Act ; The Case for a New MeV Gamma-Ray Mission: Radionuclide Astronomy in the 2020s. *Astro2020 White Paper*, 51(3):2, May 2019.

[8] Carolyn Kierans, John F. Beacom, Steve Boggs, et al. Positron Annihilation in the Galaxy. *Astro2020 White Paper*, 51(3):256, May 2019.

[9] Roopesh Ojha, Haocheng Zhang, Matthias Kadler, et al. Neutrinos, Cosmic Rays, and the MeV Band. *Astro2020 White Paper*, 51 (3):431, May 2019.

[10] Bindu Rani, H. Zhang, S. D. Hunter, et al. High-Energy Polarimetry - a new window to probe extreme physics in AGN jets. *Astro2020 White Paper*, 51(3):348, May 2019.

[11] Tonia Venters, Marco Ajello, Terri J. Brandt, et al. Energetic Particles of Cosmic Accelerators II: Active Galactic Nuclei and Gamma-ray Bursts. *Astro2020 White Paper*, 51(3): 485, May 2019.

[12] Mark McConnell, Marco Ajello, Matthew Baring, et al. Prompt Emission Polarimetry of Gamma-Ray Bursts. *Astro2020 White Paper*, 51(3):100, May 2019.

[13] Vaidehi S. Paliya, Marco Ajello, Lea Marcotulli, et al. Supermassive black holes at high redshifts. *arXiv e-prints*, art. arXiv:1903.06106, Mar 2019.

[14] Eileen Meyer, Justin Finke, George Younes, et al. Prospects for AGN Studies at Hard X-ray through MeV Energies. *Astro2020 White Paper*, 51(3):291, May 2019.

[15] Elena Orlando, Isabelle Grenier, Vincent Tatischeff, et al. Cosmic Rays and interstellar medium with Gamma-Ray Observations at MeV Energies. *Astro2020 White Paper*, 51 (3):151, May 2019.

[16] Regina Caputo, Tim Linden, John Tomsick, et al. Looking Under a Better Lamppost: MeV-scale Dark Matter Candidates. *Astro2020 White Paper*, 51(3):78, May 2019.

[17] W. B. Atwood, A. A. Abdo, M. Ackermann, et al. The Large Area Telescope on the Fermi Gamma-Ray Space Telescope Mission. *ApJ*, 697:1071–1102, June 2009. doi: 10.1088/0004-637X/697/2/1071.

[18] V. Schoenfelder et al. Instrument description and performance of the Imaging Gamma-Ray Telescope COMPTEL aboard the Compton Gamma-Ray Observatory. *Astrophys. J. Suppl.*, 86:657, 1993. doi: 10.1086/191794.

[19] D. J. Thompson et al. Calibration of the Energetic Gamma-Ray Experiment Telescope (EGRET) for the Compton Gamma-Ray Observatory. *ApJS*, 86:629–656, June 1993. doi: 10.1086/191793.

[20] F. A. Harrison et al. The Nuclear Spectroscopic Telescope Array (NuSTAR) High-energy X-Ray Mission. *ApJ*, 770:103, June 2013. doi: 10.1088/0004-637X/770/2/103.

[21] C. Winkler. The INTEGRAL mission. *Experimental Astronomy*, 6:71–76, December 1995. doi: 10.1007/BF00419260.

[22] Y. Cui, A. Bolotnikov, G. Camarda, A. Hossain, G. Yang, and R. B. James. Czt virtual frischgrid detector: Principles and applications. In *2009 IEEE Long Island Systems, Applications and Technology Conference*, pages 1–5, May 2009. doi: 10.1109/LISAT.2009.5031559.

[23] Elizabeth Hays, Alexander Moiseev, Aleksey Bolotnikov, et al. A position-sensitive high-resolution CdZnTe calorimeter for AMEGO. In *American Astronomical Society Meeting Abstracts #233*, volume 233 of *American Astronomical Society Meeting Abstracts*, page 158.26, Jan 2019.

[24] A.E. Bolotnikov, G.S. Camarda, G. De Geronimo, et al. A 4 x 4 array module of position-sensitive virtual frisch-grid cdznte detectors for gamma-ray imaging spectrometers. *Nuclear Instruments and Methods in Physics Research Section A: Accelerators, Spectrometers, Detectors and Associated Equipment*, 2018. ISSN 0168-9002. doi: https://doi.org/10.1016/j.nima.2018.07.090. URL `http://www.sciencedirect.com/science/article/pii/S0168900218309392`.

[25] Richard S. Woolf, J. Eric Grove, Bernard F. Phlips, and Eric A. Wulf. Development of a CsI:Tl calorimeter subsystem for the All-Sky Medium-Energy Gamma-Ray Observatory (AMEGO). *arXiv e-prints*, art. arXiv:1901.05828, Jan 2019.

[26] A. A. Moiseev, P. L. Deering, R. C. Hartman, et al. High efficiency plastic scintillator detector with wavelength-shifting fiber readout for the GLAST Large Area Telescope. *Nuclear Instruments and Methods in Physics Research A*, 583(2-3):372–381, Dec 2007. doi: 10.1016/j.nima.2007.09.040.

[27] A. Zoglauer, R. Andritschke, and F. Schopper. MEGAlib The Medium Energy Gamma-ray Astronomy Library. *New Astronomy Reviews*, 50(7-8):629–632, Oct 2006. doi: 10.1016/j.newar.2006.06.049.

[28] I. Antcheva, M. Ballintijn, B. Bellenot, et al. ROOT — A C++ framework for petabyte data storage, statistical analysis and visualization. *Computer Physics Communications*, 180(12):2499–2512, Dec 2009. doi: 10.1016/j.cpc.2009.08.005.

[29] S. Agostinelli et al. GEANT4: A Simulation toolkit. *Nucl. Instrum. Meth.*, A506:250–303, 2003. doi: 10.1016/S0168-9002(03)01368-8.

[30] A. C. Zoglauer. *First light for the next generation of Compton and pair telescopes : Development of new techniques for the data analysis of combined Compton and pair telescopes and their application to the MEGA prototype.* PhD thesis, Garching: Max-Planck-Institut für Extraterrestrische Physik, 2006, MPE Report, No. 289, 2006.

[31] P. F. Bloser et al. MEGA: a medium-energy gamma-ray astronomy mission concept. In Oswald H. W. Siegmund, editor, *UV, X-Ray, and Gamma-Ray Space Instrumentation for Astronomy XIV*, volume 5898, pages 34 – 45. International Society for Optics and Photonics, SPIE, 2005. doi: 10.1117/12.617315. URL `https://doi.org/10.1117/12.617315`.

[32] D. E. Gruber et al. The spectrum of diffuse cosmic hard x-rays measured with heao-1. *Astrophys. J.*, 520:124, 1999. doi: 10.1086/307450.

[33] M. Ackermann et al. The spectrum of isotropic diffuse gamma-ray emission between 100 MeV and 820 GeV. *Astrophys. J.*, 799:86, 2015. doi: 10.1088/0004-637X/799/1/86.

[34] F. Acero et al. Development of the Model of Galactic Interstellar Emission for Standard Point-source Analysis of Fermi Large Area Telescope Data. *ApJS*, 223:26, April 2016. doi: 10.3847/0067-0049/223/2/26.

[35] A. W. Strong, I. V. Moskalenko, and O. Reimer. Diffuse Continuum Gamma Rays from the Galaxy. *ApJ*, 537:763–784, July 2000. doi: 10.1086/309038.

[36] Sean Griffin and the AMEGO Team. Development of a Silicon Tracker for the All-sky Medium Energy Gamma-ray Observatory Prototype. *arXiv e-prints*, art. arXiv:1902.09380, Feb 2019.

[37] Peter F. Bloser, F. Schopper, R. Andritschke, et al. Development of silicon strip detectors for a medium energy gamma-ray telescope. *Nucl. Instrum. Meth.*, A512:220–228, 2003. doi: 10.1016/S0168-9002(03)01897-7.

[38] E. A. Wulf, B. F. Phlips, W. N. Johnson, J. D. Kurfess, and E. I. Novikova. Thick silicon strip detector compton imager. *IEEE Transactions on Nuclear Science*, 51(5):1997–2003, Oct 2004. ISSN 1558-1578. doi: 10.1109/TNS.2004.835904.

[39] Emerson Vernon, Gianluigi De Geronimo, Aleksey Bolotnikov, et al. Front-end ASIC for Spectroscopic Readout of Virtual Frisch-Grid CZT Bar Sensors. *arXiv e-prints*, art. arXiv:1904.01529, Apr 2019.

[40] A. Moiseev, A. Bolotnikov, C. Kierans, E. A. Hays, and D. Thompson. Modular Position-sensitive High-resolution Calorimeter for Use in Space Gamma-ray Instruments Based on Virtual Frisch-grid CdZnTe Detectors. In *36th International Cosmic Ray Conference (ICRC2019)*, volume 36 of *International Cosmic Ray Conference*, page 584, Jul 2019.

[41] John Tomsick, Andreas Zoglauer, Clio Sleator, et al. The Compton Spectrometer and Imager. In *Astro2020 White Paper*, volume 51, page 98, Sep 2019.

[42] G. Kanbach, R. Andritschke, F. Schopper, V. Schönfelder, A. Zoglauer, et al. The MEGA project. *New Astronomy Reviews*, 48(1-4):275–280, Feb 2004. doi: 10.1016/j.newar.2003.11.056.

[43] V. Schoenfelder, H. Aarts, K. Bennett, et al. Instrument Description and Performance of the Imaging Gamma-Ray Telescope COMPTEL aboard the Compton Gamma-Ray Observatory. *ApJS*, 86:657, Jun 1993. doi: 10.1086/191794.

[44] C. A. Kierans, S. E. Boggs, A. Lowell, et al. *Calibration of the Compton Spectrometer and Imager in preparation for the 2014 balloon campaign*, volume 9144 of *Society of Photo-Optical Instrumentation Engineers (SPIE) Conference Series*, page 91443M. 2014. doi: 10.1117/12.2055250.

[45] M. Ackermann, M. Ajello, A. Albert, et al. The fermi large area telescope on orbit: Event classification, instrument response functions, and calibration. *The Astrophysical Journal Supplement Series*, 203(1):4, oct 2012. doi: 10.1088/0067-0049/203/1/4. URL `https://doi.org/10.1088/0067-0049/203/1/4`.

[46] C. Sleator, A. Zoglauer, A.W. Lowell, et al. Benchmarking simulations of the compton spectrometer and imager with calibrations. *Nuclear Instruments and Methods in Physics Research Section A: Accelerators, Spectrometers, Detectors and Associated Equipment*, 946:162643, 2019. ISSN 0168-9002. doi: https://doi.org/10.1016/j.nima.2019.162643. URL `http://www.sciencedirect.com/science/article/pii/S0168900219311349`.

[47] Andrei Kounine et al. The alpha magnetic spectrometer on the international space station. *International Journal of Modern Physics E*, 21:1230005, 2012. doi: 10.1142/S0218301312300056.

[48] Maurice Bourquin. The ams tracking detector for cosmic-ray physics in space. *Nuclear Instruments and Methods in Physics Research Section A: Accelerators, Spectrometers, Detectors and Associated Equipment*, 541(1): 110 – 116, 2005. ISSN 0168-9002. doi: https://doi.org/10.1016/j.nima.2005.01.046. URL `http://www.sciencedirect.com/science/article/pii/S0168900205000586`. Development and Application of Semiconductor Tracking Detectors.

[49] Motohide Kokubun et al. Hard X-ray imager (HXI) for the NeXT mission. In Martin J. L. Turner and Kathryn A. Flanagan, editors, *Space Telescopes and Instrumentation 2008: Ultraviolet to Gamma Ray*, volume 7011, pages 235 – 244. International Society for Optics and Photonics, SPIE, 2008. doi: 10.1117/12.788290. URL `https://doi.org/10.1117/12.788290`.

[50] M. Casolino et al. Launch of the space experiment PAMELA. *Advances in Space Research*, 42(3):455–466, Aug 2008. doi: 10.1016/j.asr.2007.07.023.

[51] S. Straulino, O. Adriani, L. Bonechi, M. Bongi, G. Castellini, R. D'Alessandro, A. Gabbanini, M. Grandi, P. Papini, S.B. Ricciarini, P. Spillantini, F. Taccetti, M. Tesi, and E. Vannuccini. The pamela silicon tracker. *Nuclear Instruments and Methods in Physics Research Section A: Accelerators, Spectrometers, Detectors and Associated Equipment*, 530(1):168 – 172, 2004. ISSN 0168-9002. doi: https://doi.org/10.1016/j.nima.2004.05.067. URL `http://www.sciencedirect.com/science/article/pii/S0168900204010538`. Proceedings of the 6th International Conference on Large Scale Applications and Radiation Hardness of Semiconductor Detectors.

[52] Motohide Kokubun et al. Hard x-ray imager (HXI) for the ASTRO-H Mission. In Monique Arnaud, Stephen S. Murray, and Tadayuki Takahashi, editors, *Space Telescopes and Instrumentation 2010: Ultraviolet to Gamma Ray*, volume 7732, pages 320 – 332. International Society for Optics and Photonics,

SPIE, 2010. doi: 10.1117/12.857933. URL https://doi.org/10.1117/12.857933.

[53] S. D. Barthelmy et al. The Burst Alert Telescope (BAT) on the Swift MIDEX mission. *Space Sci. Rev.*, 120:143, 2005. doi: 10.1007/s11214-005-5096-3.

[54] Fiona A. Harrison, William W. Craig, Finn E. Christensen, et al. The Nuclear Spectroscopic Telescope Array(NuSTAR) HIGH-ENERGY x-RAY MISSION. *The Astrophysical Journal*, 770(2):103, may 2013. doi: 10.1088/0004-637x/770/2/103. URL https://doi.org/10.1088%2F0004-637x%2F770%2F2%2F103.

[55] V. Bhalerao et al. The Cadmium Zinc Telluride Imager on AstroSat. *J. Astrophys. Astron.*, 38:31, 2017. doi: 10.1007/s12036-017-9447-8.

[56] D. Curtis, P. Berg, Dorothy Gordon, Peter Harvey, D. Smith, and A. Zehnder. The rhessi spacecraft instrument data processing unit. *Solar Physics*, 210:115–124, 11 2002. doi: 10.1023/A:1022474004758.

[57] S. Schanne. Observing with a space-borne gamma-ray telescope: Selected results from INTEGRAL. *J. Phys. Conf. Ser.*, 41:46–60, 2006. doi: 10.1088/1742-6596/41/1/004.

[58] Lee J. Mitchell, Bernard F. Phlips, J. Eric Grove, et al. Strontium Iodide Radiation Instrument (SIRI) – Early On-Orbit Results. *arXiv e-prints*, art. arXiv:1907.11364, Jul 2019.

[59] J. S. Perkins, J. L. Racusin, M. S. Briggs, et al. BurstCube: A CubeSat for Gravitational Wave Counterparts. In *Eighth Huntsville Gamma-Ray Burst Symposium*, volume 1962, page 4088, Oct 2016.

[60] S. N. Zhang et al. eXTP – enhanced X-ray Timing and Polarimetry Mission. *Proc. SPIE Int. Soc. Opt. Eng.*, 9905:99051Q, 2016. doi: 10.1117/12.2232034.

[61] Y. Asaoka et al. The CALorimetric Electron Telescope (CALET) on the International Space Station: Results from the First Two Years On Orbit. *J. Phys. Conf. Ser.*, 1181(1): 012003, 2019. doi: 10.1088/1742-6596/1181/1/012003.